International Journal of Biological Macromolecules 183 (2021) 528–548

Contents lists available at ScienceDirect

International Journal of Biological Macromolecules

journal homepage: http://www.elsevier.com/locate/ijbiomac

Poly-L-Lysine inhibits VEGF and c-Myc mediated tumor-angiogenesis and induces apoptosis in 2D and 3D tumor microenvironment of both MDA-MB-231 and B16F10 induced mice model

Souvik Debnath [a,b], Avinaba Mukherjee [c], Dhananjoy Saha [d], Jyotirmayee Dash [e], Tapan Kumar Chatterjee [b,f,*]

[a] Department of Basic Medical Sciences, Purdue University, 625 Harrison St, West Lafayette, IN-47907, USA
[b] Division of Pharmacology Research Laboratory, Department of Pharmaceutical Technology, Jadavpur University, Jadavpur-700032, India
[c] Department of Zoology, Charuchandra College, University of Calcutta, Kolkata-700029, India
[d] Deputy Director, Technical Education, West Bengal State Council & Technical Education, Bikas Bhavan, Saltlake, Kolkata, West Bengal, India
[e] School of Chemical Sciences, Indian Association for the Cultivation of Science, Jadavpur, Kolkata-700032, India
[f] Department of Pharmaceutical Science and Technology, JIS University, Kolkata, India; and Former Professor, Division of Pharmacology, Department of Pharmaceutical Technology, Former Director, Clinical Research Centre, Jadavpur University, Kolkata, India

ARTICLE INFO

Article history:
Received 14 January 2021
Received in revised form 16 April 2021
Accepted 17 April 2021
Available online 21 April 2021

Keywords:
Poly-L-lysine (PLL)
3D tumor-microenvironment
Apoptosis
VEGF
Caspase-3

ABSTRACT

Cancer is a widespread disease that has shown promising mortality worldwide. Our previous study has been shown the efficacy of Poly-L-lysine (PLL) as a promising cytotoxic effect against cancer cells. However, exact-mechanism of PLL in 3D physiological relevant tumor-microenvironment and against tumor-angiogenesis has never been analysed. In this study, we have investigated apoptotic efficacy of PLL, if any in opposition to proliferative aggressive cancer cell MDA-MB-231 both 2D and-3D cell culture conditions. Furthermore, PLL was administered in B16F10 murine melanoma cells induced BALB/c mice model. The study has been designed through transcription and translation level of PLL-induced tumor-angiogenesis and apoptotic gene-expression modulation level and various relevant histological studies in comparison with untreated control. Studies have shown anti-proliferative and anti-tumor angiogenic efficacy of PLL better in *in-vitro* 3D tumor-microenvironment against MDA-MB-231 breast cancer cells. Furthermore, *in-vivo* model, PLL was found to suppress tumorigenesis process at minimum dose. PLL found to induce apoptosis through-upregulation of cytosolic-cytochrome-C, caspase-3 and PARP activations when administered in B16F10 induced *in-vivo* tumor. In blocking proliferation and tumor-angiogenesis, PLL was found to be effective as it significantly downregulated activity of VEGF, VEGFR2, Ki-67 and c-Myc expression. As PLL blocked tumor progression and induced DNA-break, also upregulated apoptotic process and recovered tissue architecture as revealed from histological study in comparison with untreated control. Overall PLL was found to be a promising anti-tumor angiogenic and anti-proliferative drug that was effective both in *in-vitro* breast cancer 3D tumor-microenvironment and *in-vivo* metastatic-mice-model.

1. Introduction

Promising worldwide mortality due to cancer is found to increase now a day. Regarding the anticancer drug development, several studies have been made [1,2]. According to WHO, nearly 21.4 million new cancer cases, and more than 13.2 million deaths are projected to occur worldwide by the year 2030 [3,4]. In combating such disease, apoptotic induction and neovascularisation inhibition in tumor cells are considered to be very useful [5]. However, most of the currently available anti-cancer drugs fail to differentiate between normal and neoplastic cells and as a result, they lack target specificity [5,6]. Therefore, target specific anti-cancer drug is highly solicited, now a day. Our previous studies have shown the efficacy of Poly-L-lysine (PLL) as a promising anticancer drug. However, the exact mechanism of PLL in both 2D and 3D tumor microenvironments and against angiogenesis has never been analysed.

Angiogenesis plays a significant role in the tumor progression and metastatic progression [7] refers to three distinct phases including the extracellular matrix destruction, uncontrolled cell proliferation, and cellular invasion [8,9]. Theoretically, tumor growth can be suppressed if the inhibition of angiogenesis can be done so that new blood vessel

* Corresponding author at: Prof. (Dr) Tar Chatterjeepan Kuma, Dean, Department of Pharmaceutical Science and Technology, JIS University, Kolkata, India; and Former Professor, Division of Pharmacology, Department of Pharmaceutical Technology, Former Director, Clinical Research Centre, Jadavpur University, Kolkata, India.
E-mail addresses: souvik123456@gmail.com (S. Debnath), dr.tkchatterjee@jisuniversity.ac.in, crctkc@gmail.com (T.K. Chatterjee).

https://doi.org/10.1016/j.ijbiomac.2021.04.109
0141-8130/

cannot be formed [10]. Induction of aberrant angiogenesis represents a shared hallmark in several chronic inflammatory diseases including diabetes, cardiovascular diseases, and cancer [11]. Bigger attention has been addressed to prevent cancer by suppressing angiogenesis, leading to the concept of angio-prevention [12]. Currently, the anti-angiogenic agents target the vascular endothelial growth factor (VEGF) pathway [13]. However, most clinically employed antiangiogenic drugs are only effective in a subset of patients but in them usually, relapse occurs. Therefore, the identification of new anti-angiogenic compounds that could overcome these drawbacks is urgently needed.

Angiogenic molecular suppression if are needful in lowering the proliferation of cancer cells can also be made into consideration. Besides this, major regulation in pro and anti-apoptotic proteins like Bax/Bcl2 regulation through downregulation of angiogenesis and proliferation through our proposed molecule PLL will also be verified to establish PLL to be a major target specific apoptotic molecule against tumorigenesis.

Poly-L-lysine (PLL) has potent anti-tumor activity particularly against Ehrlich ascites carcinoma (EAC), Sarcoma-180, DAL, HeLa, and Lewis lung carcinoma *in-vitro* and *in-vivo* tumor model [14–16]. Previously PLL induced regression of tumor neovessels was reported which was supposed to be done by the interference with the signalling of vascular endothelial cadherin. In addition, with this, previous studies from our group also revealed that induction of apoptosis by modulating the expression of cell cycle-regulatory, caspase-3 apoptotic pathway by PLL. Additionally, PLL exhibits enhanced antitumor actions as a carrier of anticancer drugs, when applied to HeLa, and L1210 murine leukemia cells. Our previous biological investigation also has shown retardation of cell proliferation and antitumor angiogenic property in the *in-vivo* EAC, Sarcoma-180, and DAL tumor models without any toxic side effects [14,15].

Here in the experimental research, to establish if PLL is a major antitumorigenic compound, we have used metastatic human breast cancer MDA-MB-231 and the murine melanoma cancer B16F10 cells as our *in-vitro* and *in-vivo* experimental models. Both the cell line used in the present study are relevant in evaluating the prevention of cellular metastasis, because, as clinically cells from both types of cancers are known to metastasize and are derived as the clonal population of cells acquired with stem cell properties and with a heterogeneous population. Also, they can give rise to both types of luminal and basal-like progenitors. The cancer stem cell arises by clonal evolution as a result of selection for the cell with the highest fitness in the neoplasm in addition to other organs.

The cellular conditions in monolayer culture (2D) *in-vitro* differ significantly from *in-vivo* conditions since the tumor population is heterogeneous and consists of a differential microenvironment for the cells at different stages of development and differentiation. Also, in natural conditions, cells in the tumor interact with adjacent cells and the extracellular matrix, and also have different access to nutrients and oxygen [17]. Often these differences are the cause of the ineffectiveness of antitumor therapy, which showed promising results in preclinical studies in 2D cell growth conditions *in-vitro*. An alternative model for the study of tumor cell susceptibility to antitumor agents is spherical 3D cultures or multicellular tumor spheroids (MCTs) [18,19]. Cells in 3D culture actively interact with each other, the extracellular matrix, and the microenvironment. MCTs consist of cells that are at different stages of their development and under different influences (proliferative, apoptotic, and anti-angiogenic effect) [20,21]. Due to their structure, MCTs are important for testing the therapeutic effect of antitumor drugs, as well as for assessing the invasive capacity of transformed cells. Based on this phenomenon, the present study aims to evaluate the effect of PLL on the proliferation, and apoptotic effect of MDA-MB-231 epithelial aggressive breast cancer cells in 2D and 3D tumor microenvironments.

Nevertheless, the molecular mechanism behind the anti-angiogenic effects of PLL and its efficacy of it at tumor microenvironmental modulation remains poorly understood. As VEGF/VEGFR signalling pathway is increasingly recognized as a key regulator during tumor angiogenesis, we here investigate the effect of PLL on VEGF/VEGFR signalling. In the present study, we have shown that poly-L-lysine (PLL) effectively inhibited angiogenic processes in *in-vitro* and *in-vivo* murine melanoma B16F10 mice model, and we have tried to establish for the first time that the anti-angiogenic activity of PLL was improved by causing suppression of the tumor proliferation, c-Myc, and VEGF angiogenesis pathway. The mechanistic exploration of how PLL suppressed the protein expression of VEGF and VEGFR-2 in tumors of a B16F10 in the BALB/c mouse model along with apoptotic induction was also being evaluated.

2. Materials &methods

2.1. Chemicals & reagents

Breast cancer cell line- MDA-MB-231 and B16F10 Murine Melanoma cancer cells were obtained from NCCS, Pune. PLL hydrobromide (Mrs 30,000–70,000) and 3− (4, 5-Dimethytthiazol-2-yr) −2, 5-diphenyltetrazolium bromide (MTT) were obtained from Sigma-Aldrich (USA). Primary anti-bodies Cytochrome-*C*, cleaved caspase-3, cleaved PARP, VEGF, VEGFR2, GAPDH and secondary antibodies were acquired from Santa Cruz, CA, USA. Dulbecco's modified Eagle medium (DMEM), Roswell Park Memorial Institute medium-1640 (RPMI-1640), Penicillin, streptomycin and neomycin (PSN), fetal bovine serum (FBS), trypsin & ethylene diamine tetraacetic acid (EDTA) obtained from HI Media (India). Horseradish peroxide (HPR), Giemsa stain, Hematoxylin & Eosin were purchased from R&D Systems (USA). A primary antibody for immunohistochemistry study CD-34 and Ki-67 were obtained from R&D Systems (USA). Inc., CA USA. All water-soluble composites were liquified in Dulbecco's Modified Eagle's medium (DMEM), while unsolvable substances were liquified into dimethyl sulfoxide (DMSO) (Sigma, USA), the-concluding attentiveness of DMSO in each sample was less than 0.1%. All explanations were approved through a 0.22 μm fitter (GVMP 01230, Millipore) and stored at 4 °C until use. The additional chemicals used were of analytical grade. All solutions were passed through a 0.22 μm fitter (GVMP 01230, Millipore) and deposited at 4 °C until use.

2.2. Preparation of the drug solution

The solution of PLL was made from lyophilized PLL hydrobromide (Fig. 1A) in sterile phosphate-buffered saline (PBS, pH: 7.4). The solution was kept at 4 °C to maintain stability for extended use.

2.3. Cell culture

MDA-MB-231 (in both 2D and 3D systems), B16F10 cells remained in DMEM. Peripheral blood mononuclear cells (PBMC) were inaccessible from a healthy human donor and maintained in RPMI-1640 medium.

All the cells were fed with medium supplemented with 10% FBS and 1% antibiotics (100 U/ml penicillin and 100 μg/ml streptomycin) at 37 °C in a humidified incubator containing 5% CO_2. Adherent cells were passaged using trypsin/EDTA and phosphate-buffered saline (PBS) solution.

The maximum extensively rummage-sale cell type, though, has been the B16F10 cell line that impulsively procedures tumors subsequently biochemical introduction of melanoma in C57BL/6J mice and stretches upsurge to a miscellaneous range of sub-clones with numerous tendencies for proliferation, invasion, and metastasis. In the subcutaneous B16F10 pulmonary metastasis melanoma tumor within BALB/c mice, provide a new melanoma-bearing mice model for haploidentical lymphocytes infusion. Equally, B16F10 has the high metastatic possible to

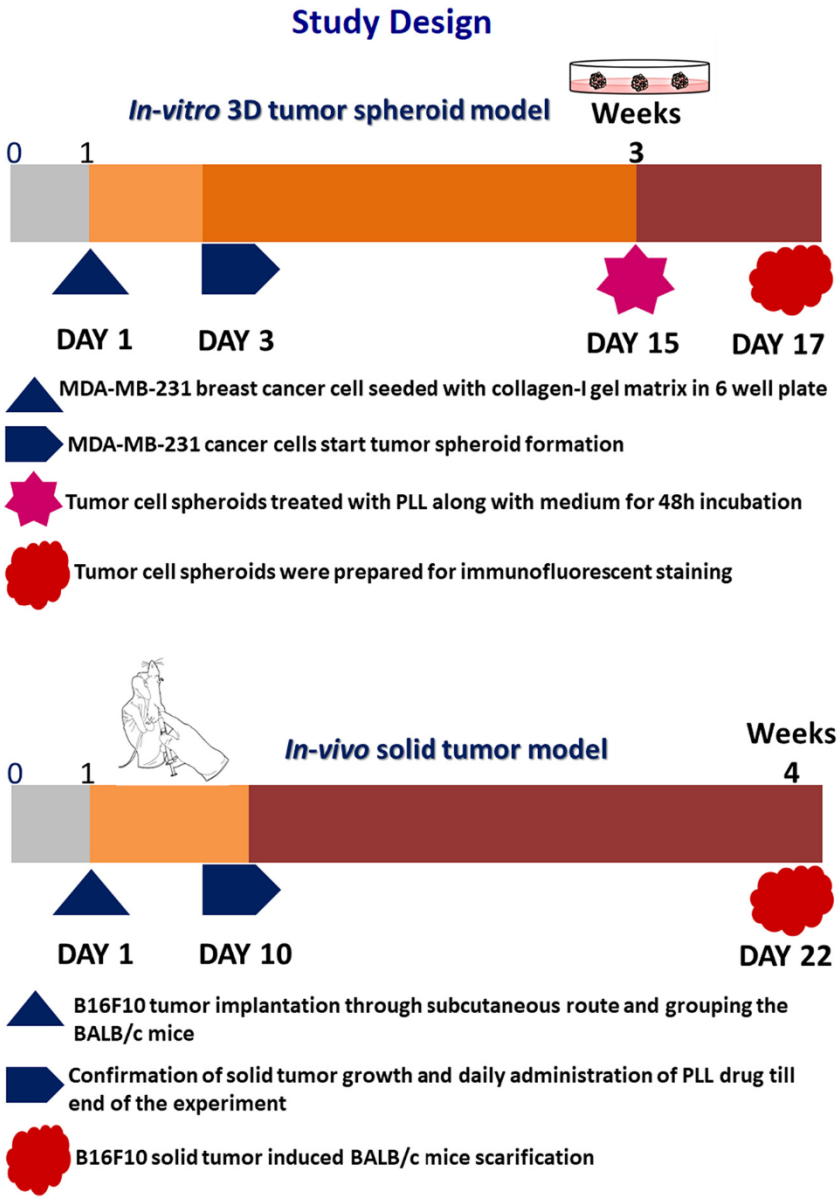

Fig. 1. Study design of *in-vitro* MDA-MB-231 3D tumor spheroid model and *in-vivo* B16F10 solid tumor BALB/c mice model schematic diagram.

unfriendly instinctual organs, maximum particularly the lungs, and has been perfect for *in-vivo* studies because of its summary development design and high turnover, persuading death within two to four weeks after SC injection into mice.

For *in-vivo* tests, the B16F10 cell was preserved in the peritoneal cavity of mice by inoculating 0.1 ml into liquid cells every 7 days. Tumor cell amounts were complete in a Neubauer hemocytometer using the trypan blue dye prohibiting technique. Cell feasibility was originated to be 95% or more. Tumor cell postponements were organized in phosphate-buffered saline (PBS).

2.4. Proliferation assay

The proliferation of MDA-MB-231 and B16F10 cells were assessed by the MTT colourimetric assay. Fleetingly, MDA-MB-231 and B16F10 cells sowed in 96-well culture plates at the compactness of 8×10^4 cells/well and gestated for 24 h. The cells were preserved with diverse absorptions of PLL (0, 1.0, 5.0, 10.0, 20.0, 30.0 & 40.0 μg/ml); control cells were preserved with PBS. At that time, the dishes were gestated at 37 °C under 5% CO_2 for 48 h. Next conduct, the supernatants detached, 100 μl of 5 mg/ml MTT key supplementary to each well, and the plate was gestated for 3 h. The hastened formazan crystals were thinned in DMSO and unhurried at 540 nm with the Bio-Rad 680 Microplate student. The reserve ratio (%) intended by the calculation and was used for more lessons.

In addition, this PBMC was inspected by proliferation assay after existence unprotected with the PLL of the same quantities. The reserve proportion (%) intended by the calculation and uttered as the regular of three equivalent tests. Morphological vicissitudes encouraged on cells by PLL experiential done upturned light microscopy (Carl Zeiss, Germany).

$$1\% = \left(1 - \frac{A\ blank\ treated - A\ blank}{A}\right) \times 100$$

2.5. Preparation of 3D tumor spheroids

Collagen I (R&D systems, USA), a 3D culture matrix was used. Type I collagen was used at a concentration of 1 mg/ml according to Paszek et al. [22]. Collagen was neutralized according to the manufacturer's protocol. Collagen gels were prepared using bovine collagen; mixed properly Matrigel™ and collagen gels were prepared using a 1:1 volume ratio of Matrigel™ and type I collagen keeping the final collagen concentration at 1 mg/ml. In this 3D-culture system, 300,000 MDA-MB-231 aggressive breast cancer cell was used to mimic the *in-vivo* physiological relevant human breast cancer tissue [23]. Cells were suspended in 3 ml collagen or a 3 ml Matrigel™-collagen mixture and seeded into 35 mm well inserts of a six-well plate [24]. The gels were allowed to solidify for 30 minutes at 37 °C before adding a combined medium onto each gel (2 ml) and into each well (10 ml). After 3 days, the MDA-MB-231 tumor cells start the spheroids formation. 3D cultures were maintained for 14 days and the medium was changed every three days. After 14 days of incubation, tumor cell spheroids were treated with PLL10 μg/ml, 20 μg/ml and 40 μg/ml concentration with medium and incubated for 48 h. After then tumor cell spheroids were prepared for immunofluorescence staining (Fig. 1).

2.6. Immunofluorescence microscopy study

MDA-MB-231 cells were cultured on coverslips for 2D monolayer culture and with collagen I for 3D culture. Cells were treated with PLL according to each condition, 2D, or 3D cultures. Cells grown on the coverslips and 3D tumor spheroids were fixed in 4% formaldehyde in PBS for 30 min. Cells were washed with PBS and then treated with 0.1% Triton-X 100 for 8 min for 2D monolayer culture and 1 h for the 3D collagen culture. Cells were washed with PBS and blocked with 3% bovine serum albumin (BSA) in PBS for 1 h at room temperature. After blocking, cells were incubated with caspase-3 and Ki-67 primary antibodies overnight at 4 °C. After washing, cells were incubated with anti-mouse secondary antibodies for 1 to 6 h at room temperature on the rocker. DAPI was used to stain nuclei. The coverslips were mounted and sealed on histological glass slides with prolong antifade reagent (Invitrogen, Camarillo, CA). The image was captured using a fluorescence microscope (Leica Germany Model DM900 fluorescent). Based on the images, the positive cell density within the 3D cell culture was calculated by counting specific marker positive cell numbers *via* ImageJ software. Three samples for each condition were used and at least three images from each sample were analysed.

2.7. Animals

Eight per cage of healthy female BALB/c mice weighing about 20 g were kept for at least 14 days in environmentally controlled room temperatures (23 ± 2 °C), humidity (50 ± 5%), and light (12 h light/dark cycle) and were given with food and water *ad libitum*. All experiments were conducted as per guidelines cleared by the Animal Ethics Committee of the Department of the Pharmaceutical Technology of Jadavpur University, India (Registration number: 147/1999/CPCSEA).

2.8. Induction of B16F10 solid murine melanoma tumor

In the B16F10 induced tumor model, 24 animals were assigned to 4 groups (8 animals per group), *e.g.*, groups I, II, III, IV, respectively. Ascites fluid was drawn out from B16F10 tumor-bearing C57BL6 mouse at the log phase (day 7–8 of tumor-bearing) of the tumor cells.Each group was given subcutaneous inoculation (s.c.) of 0.1 ml B16F10 cell suspension containing 2×10^6 cells/ml. Group-I served as the B16F10 control, followed by treatments groups-II and III, receiving doses of (20 and 40 mg/kg of b.w) of PLL (i.p), respectively. Group-IV received 5-FU, as the reference drug (20 mg/kg i.p.). PLL treatment was started 10 days after tumor inoculation and was continued for 21 days. The tumor volume was determined by direct measurement with Vernier calipers every 2 days after the tumor implantation and the tumor inhibition was calculated. On day 22, the animals were sacrificed by cervical dislocation and the tumors were removed for evaluation of various antitumor activities (Fig. 1).

2.9. Acute toxicity assay for drug dose selection in in-vivo assay

For drug dose selection mice ($n = 6$) were injected by PLL only at a dose of 10, 20, 40, 80 mg/kg b.w. Acute toxicity was monitored between them. As an indicator of acute toxicity, thirst generation and rapid movement was observed.

2.10. Tumor volume

The proportion of the emerging tumors was unhurried with Vernier calipers at 2-day intermissions for 21 days and the tumor volume was intended with the method:

$$V = \pi/6 \times (D_1) \times (D_2)^2$$

Where D_1 is the extended diameter and D_2 is the petite length.

2.11. Tumor weight

After 21 days, all tumors (2 discs/animals) remained stamped out, considered directly, and the average weights were intended. All tumors were expunged and alienated into two portions. The first serving was cast-off for the documentation of protein appearance heights, and the second was used for histopathological and immune-histochemical capacities. The fraction reserve was intended by the formulation:

$$\%\text{Inhibition} = 1 - B/A \times 100.$$

Where A is the average weight of the control group and B is the average tumor weight of the preserved group.

2.12. Determination of mean survival time (MST) and percentage increase in lifespan (%ILS)

After expense, 3 mice from the respective group were experiential for mean survival time (MST). The animal existences were logged for up to 50 days. The consequence of PLL on the percentage increase lifespan (%ILS) was intended grounded on the humanity of the investigational mice. Humanity was observed by recording (% ILS) and (MST) as per the subsequent formulation:

$$\%\text{ILS} = \frac{\text{MST of treated animals}}{\text{MST of control animals}} \times 100 - 100$$

2.13. Estimation of haematological and serum biochemical parameters

After 21 days from the onset of the experimentation, animals were sacrificed by cervical dislocation and blood samples remained composed from the heart using heparinized syringes for haematological and serum biochemical constraints.

2.14. Histopathology of liver and kidney tissue

Three arbitrarily designated BALB/c mice from each group were foregone and their liver and kidney tissues isolated. Post-isolation from obeying tissue matter, the livers remained to wash away with brackish and weighed, cut into small smithereens, fixed in 10% buffered formalin, desiccated in snowballing concentrations of ethanol, cleared in xylene,

and embedded in paraffin wax. Sections (5 to 6 μm thick) were cut, tainted through hematoxylin and eosin (H&E), and inspected underneath a light microscope (Eclipse TS100, Nikon, Japan).

2.15. H&E staining of a B16F10 solid tumor tissue section

On day 22, BALB/c mice from each cluster selected arbitrarily and sacrificed them correctly by cervical dislocation, after then tumors that established at the site of inoculation stayed expunged and immovable in 10% formaldehyde and fixed in paraffin and 5 μm pieces were blemished with H&E staining. All the slides stayed inspected for histopathological vicissitudes for any alteration by means of light microscopy. Three animals each cluster remained rummage-sale for histological and immune-histochemical investigation.

2.16. Study of the morphological changes of B16F10 tumor cells by Giemsa staining method

On day 22, the animals were sacrificed by cervical dislocation and the tumors detached. Then B16F10 tumor tissue segments were immovable on clean glass slides, air-dried, and fixed in a solution of methanol/ acetic acid (3:1). The slides remained hydrated with PBS & stained with 0.1% Giemsa solution and pragmatic beneath a complex light microscope (Eclipse TS100, Nikon, Japan).

2.17. Immunohistochemistry analysis

Dense tumor segments (~5 μm) were used aimed at the immune-histochemical examination of Ki-67, and CD34 proteins. Fleetingly, the segments were hydrated in 1× PBS for 5 min. Antigen recovery was done by raising the pieces in 10 mM sodium citrate buffer (pH 6.0) at 80 °C for 10 min. The pieces were chilled to room temperature for 20 min. Subsequent a 5-min rinse with 1× PBS, the endogenous peroxides were blocked by 1% hydrogen peroxide in PBS for 5 min. The pieces were eroded as before and blocked for 1 h. in PBS comprising 1.5% normal serum. The samples were raised overnight by primary antibodies correspondingly in contradiction of Ki-67 & CD34 at 4 °C in a moistened compartment. After washing by PBS, the slices stayed gestated with horseradish peroxides (HRP) – conjugated secondary antibodies at 1:100 watering for 30 min. at 37 °C. The immune responses were

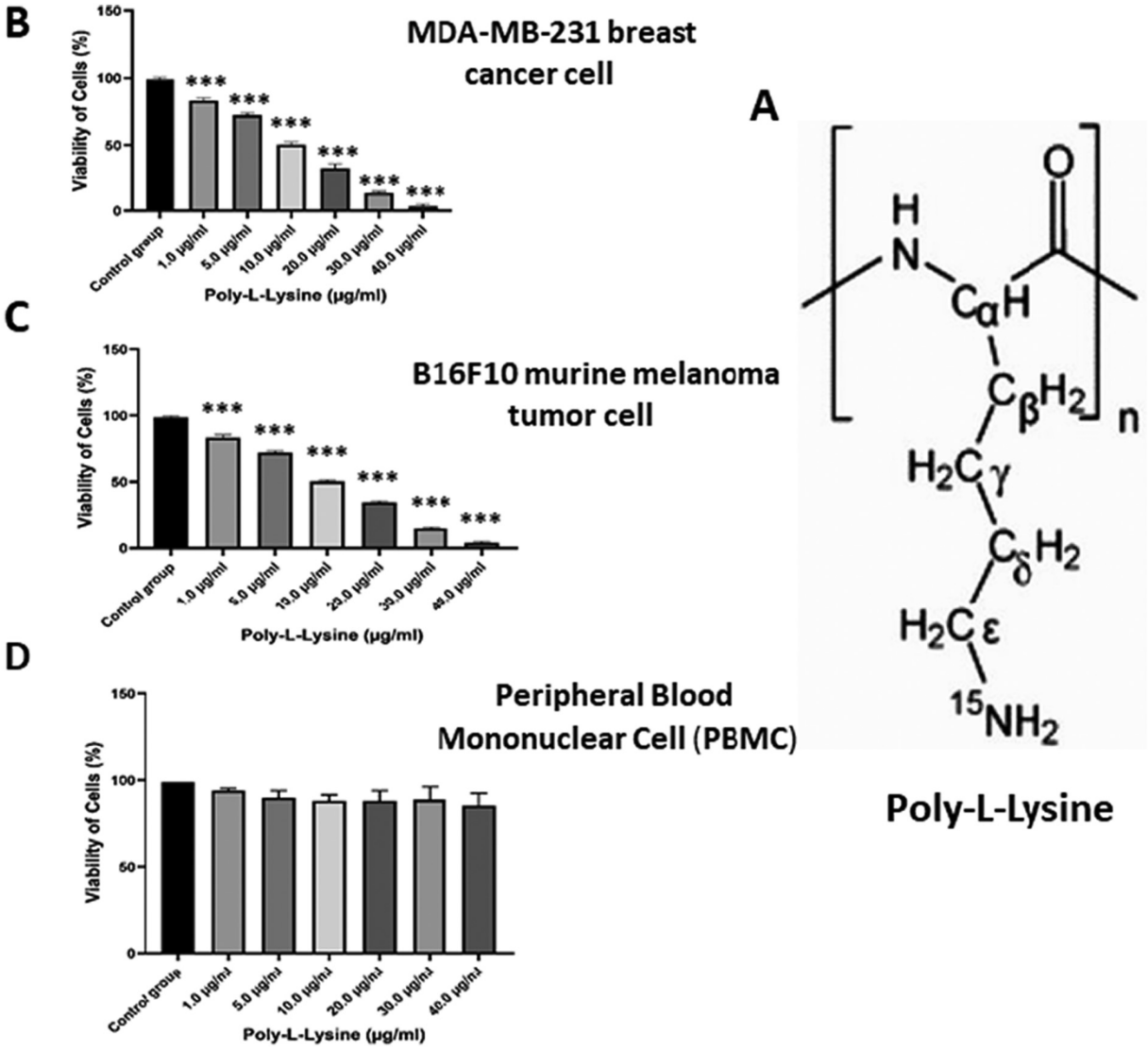

Fig. 2. Chemical structure of poly-L-lysine (PLL) (A). PLL inhibits cell proliferation in MDA-MB-231 aggressive breast cancer cells, B16F10 murine melanoma tumor cells and PBMC cells. MDA-MB-231 (B) and B16F10 (C) cells were exposed to various concentrations of PLL at various doses for 48 h and cell proliferation assays were performed. Data are exposed as mean ± SEM, $n = 3$. MDA-MB-231: epithelial human breast cancer cell; B16F10: murine melanoma tumor cell; PBMC: Peripheral Blood Mononuclear Cell.

envisaged by submerging the transparencies in 3, 3′-diaminobenzidine tetrahydrochloride mixture. The pieces remained counterstained by hematoxylin. Negative control sections were treated with the oversight of the primary antibodies. All sections were arid, equestrian observed under an alight microscope (Eclipse TS100, Nikon, Japan), and photographed (10×).

2.18. Western blot analysis

B16F10 solid tumor remained collected from control and PLL drug-treated mice. At the culmination of the conduct, tumor tissues remained homogenized in the RIPA buffer kit is the attendance of protease inhibitors. Cell lysates were composed, and the total protein filling assessed by the Lowry method. The protein (30 μg) innards from the cell lysates were detached by 10% SDS–PAGE and transported to a nitrocellulose membrane. The membranes were gridlocked, wash away and the particular membranes were investigated using antibodies for VEGF, VEGFR2, and GAPDH immediate at chamber malaise. GAPDH was occupied as the housekeeping gene. The blots remained to bear away and immunoreactive bands stayed gestated with a 1:2000 weakening of HRP (horseradish peroxidase) conjugated secondary antibody for 2 h at room temperature. Compulsory signals were imagined with TMB (3, 3′, 5, 5' Tetramethylbenzidine) substrate. Comparative band concentrations were strong-minded Image-J software.

2.19. Chicken chorioallantoic membrane (CAM) assay

The CAM assay delivers an exclusive prototypical for inspecting the development of new blood vessel formation and vessel retorts to anti-angiogenic agents. Using this perfect, we inspected the *in-vivo* anti-angiogenic commotion of PLL. The anti-angiogenic consequence of PLL was deliberate by with CAM angiogenesis in impregnated eggs, *in-vivo*. Groups of 10 fertilized chicken eggs remained transported to an egg incubator, incubated at 37.8 °C and 60–70% relative humidity for 8 days. After gestation, an unimportant hole was punctured on the comprehensive end of the egg and an opening was prudently shaped on the eggshell. Sterilized filter paper disks (5 × 5 mm) soaked with PLL (10, 20, and 40 μg/ml) was located on the CAM. The holes were then enfolded with cellophane duct tape. After gestated for extra 2 days, the CAMs were photographed. Variations in the vascularization pattern were inspected. Angiogenesis was enumerated by manually including the number of blood vessel branch points.

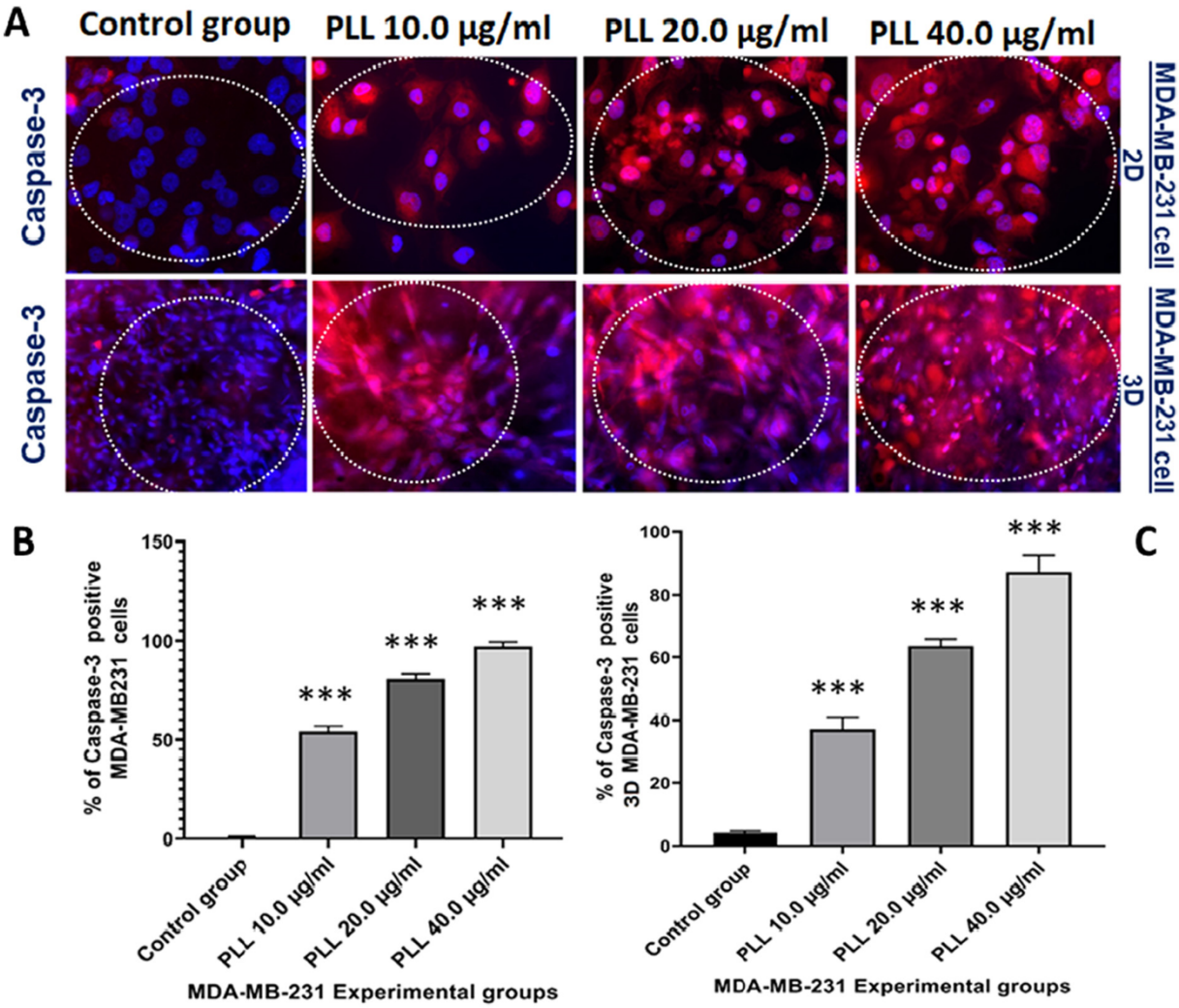

Fig. 3. Caspase-3 immunofluorescence assay of cells in 2D and 3D MDA-MB-231 collagen-I culture model. For detection of caspase 3 MDA-MB-231 cells stained with DAPI (blue), anti-caspase-3 antibodies (red). (A)Caspase-3 was detected in all treated groups, yet the MDA-MB-231 control group did not alter expression. Here, caspase-3 positive MDA-MB-231 cells were co-stained to detect cleaved caspase-3 protein expression in apoptotic cells. The caspase-3 red signal represents the cleaved caspase-3 levels (200× magnification). Nuclear was demonstrated using DAPI staining. (B) and (C) The graphs represent the means ± SEM of cleaved caspase-3 positive apoptotic cells. Scale bars represent 25μm. $^{***}P < 0.001$ compared with the control.

2.20. Cell perfusion and FACS analysis for apoptosis detection

After inducing tumor by B16F10, cells were perfused in RPMI-1640 medium by using the perfusing buffer as made by the manufacturer's protocol. The perfused cell was isolated by using nylon mesh.

Apoptosis in the B16F10 cells (6×10^5 cells/ml in a 12-well plate) was assessed by annexin-V-fluorescein isothiocyanate (annexin-V-FITC) and propidium iodide (PI) discolouration by using the BD Bioscience, Annexin V-FITC Apoptosis detection kit. Fleetingly, cells were harvested and eroded twice with PBS. The supernatant was castoff, and the pellets were bear away in 100 μl of the compulsory buffer. Subsequent a gentle vortex, next the cells were hatched for 15 min on ice in the dark with a mixture of 5 μl of annexin-V-FITC and 5 μl of PI. Cells were hatched 10 min at room temperature in the dark and additional analysed by FACS Calibur flow cytometer (Becton Dickinson, USA) using the supplied software in the instrument (BD Cell Quest software).

2.21. Reverse transcriptase PCR analysis

Total RNA from *in-vitro* MDA-MB-231 drug-treated, and control cells was extracted using TRIzol (Invitrogen, USA) according to the manufacturer's protocol and was reverse transcription reagent conferring to the manufacturer's instruction. Here 2 μg of total RNA from MDA-MB-231 drug-treated ware used for reverse-transcription reactions with or without reverse transcriptase. On the other side, from the *in-vivo* B16F10 solid tumor tissues were gathered from control and drug-treated mice. At the termination of the behaviour period, tumor tissues were standardized in RIPA buffer kit is the occurrence of RNase inhibitors. Cell lysates were composed for quantitative Real-Time Reverse transcription-polymerase Chain Reaction (Real-Time RT-PCR). Total RNA was removed, reverse transcribed, and enlarged by PCR using QIAamp RNA Blood Mini Kits (QIAGEN) subsequent the commands of the constructer. From the cells, lysed total RNAs were inaccessible using TRIzol (Invitrogen, USA) rendering to the constructer's commands. Languages of VEGF and c-Myc were scrutinized by the PCR technique using gene-specific primers. Responses were gestated at 94 °C for 2 min and were then augmented using temperature strictures of 94 °C for 30 s, 60 °C for 30 s, and 72 °C for 30 s. Intensifications were carried out for 35 cycles, shadowed by a 7-min postponement at 72 °C temperature. All the data were consistent with the glyceraldehyde-3-phosphate dehydrogenase (GAPDH) gene.

2.22. Statistical analysis

All the consequences standards were articulated as a mean ± standard error of the mean (SEM). Investigational consequences were analysed by student's *t*-test and one-way analysis of variance (ANOVA) using SPSS statistical software. $^{*}P < 0.05$,$^{**}P < 0.01$, and $^{***}P < 0.001$ were statistically significant when associated with control.

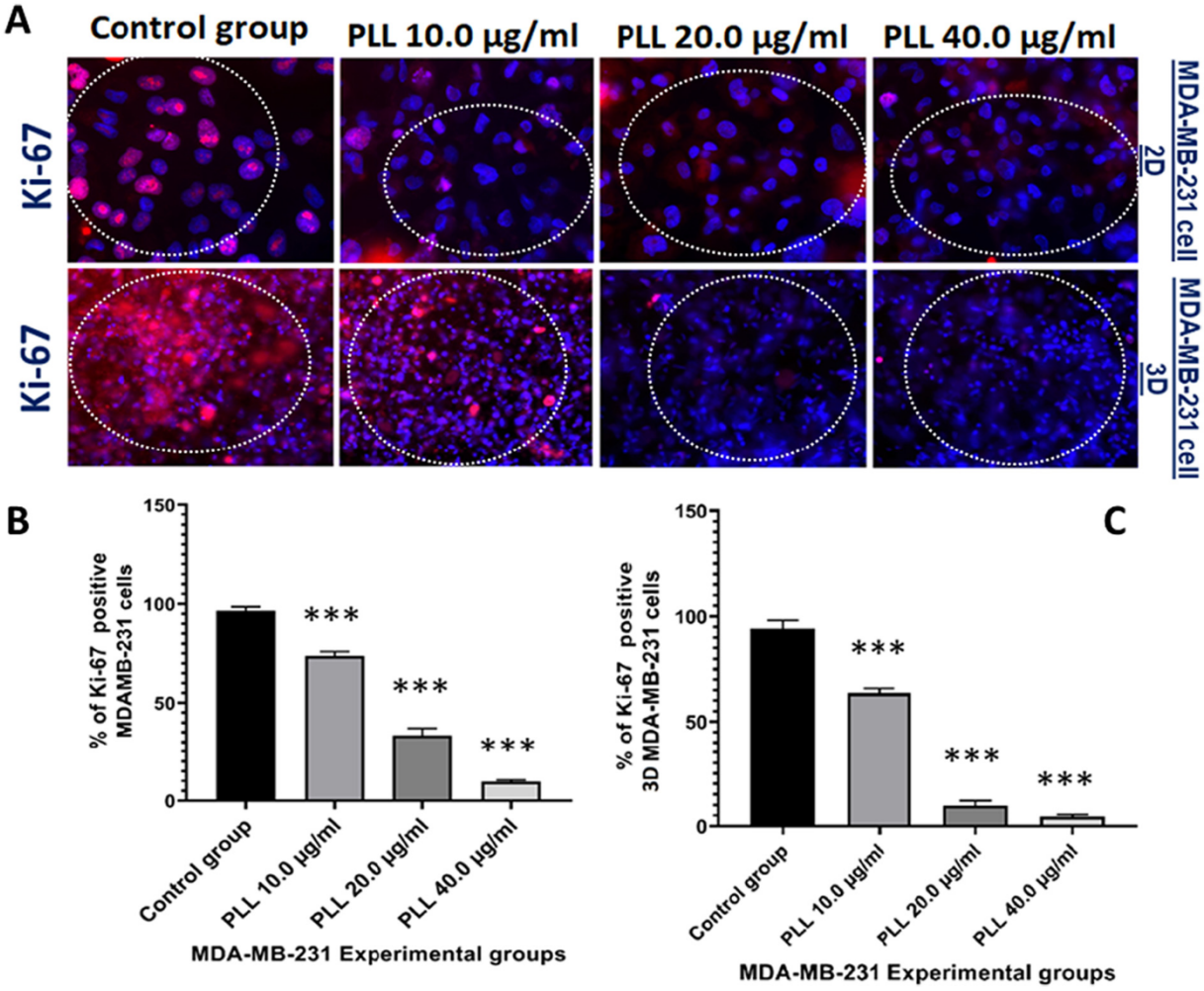

Fig. 4. Ki-67 immunofluorescence assay of cells in 2D and 3D MDA-MB-231 collagen-I culture model. For detection of Ki-67 MDA-MB-231 cells stained with DAPI (blue), anti-Ki-67 antibodies (red). (A) The Ki-67 red signal represents tumor cell proliferation levels (x200 magnification). Proliferation (red) and nuclei (blue) are indicated by Ki67 and DAPI staining, respectively. Percentage of cells with Ki-67 positive nuclei in PLL treated MDA-MB-231 cell reduced dose-dependently. In each experiment at least 150 cells were included in the calculation. Tumor proliferation in MDA-MB-231 cells grown in 2D and 3D culture detection (red), nuclear staining with DAPI (blue). Scale bars indicate 25 μm. (B) and (C) The graphs represent the means ± SEM of Ki-67 positive cells. Scale bars represent 25μm. $^{***}P < 0.001$ compared with the control.

3. Results

3.1. Poly-L-Lysine (PLL) inhibits the proliferation of in-vitro MDA-MB-231 and B16F10 cancer cells

To inspect the consequence of PLL on the proliferation of MDA-MB-231 and B16F10 cells were preserved by diverse concentrations of PLL (0, 1.0, 5.0, 10.0, 20.0, 30.0 and 40.0 μg/ml) for 48 h, and their propagation was unhurried. After 48 h of experience, 0.5 μg/ml PLL did not damage the active proliferation. Though, an attentiveness of 1.0–40.0 μg/ml it effectively lessened the cell proliferation 10.2%–84.7% correspondingly, as associated with the control group (Fig. 2). The IC_{50} value was determined and found to be 11 μg/ml and 10 μg/ml for MDA-MB-231 and B16F10 respectively. The proliferation of MDA-MB-231 and B16F10 cells was

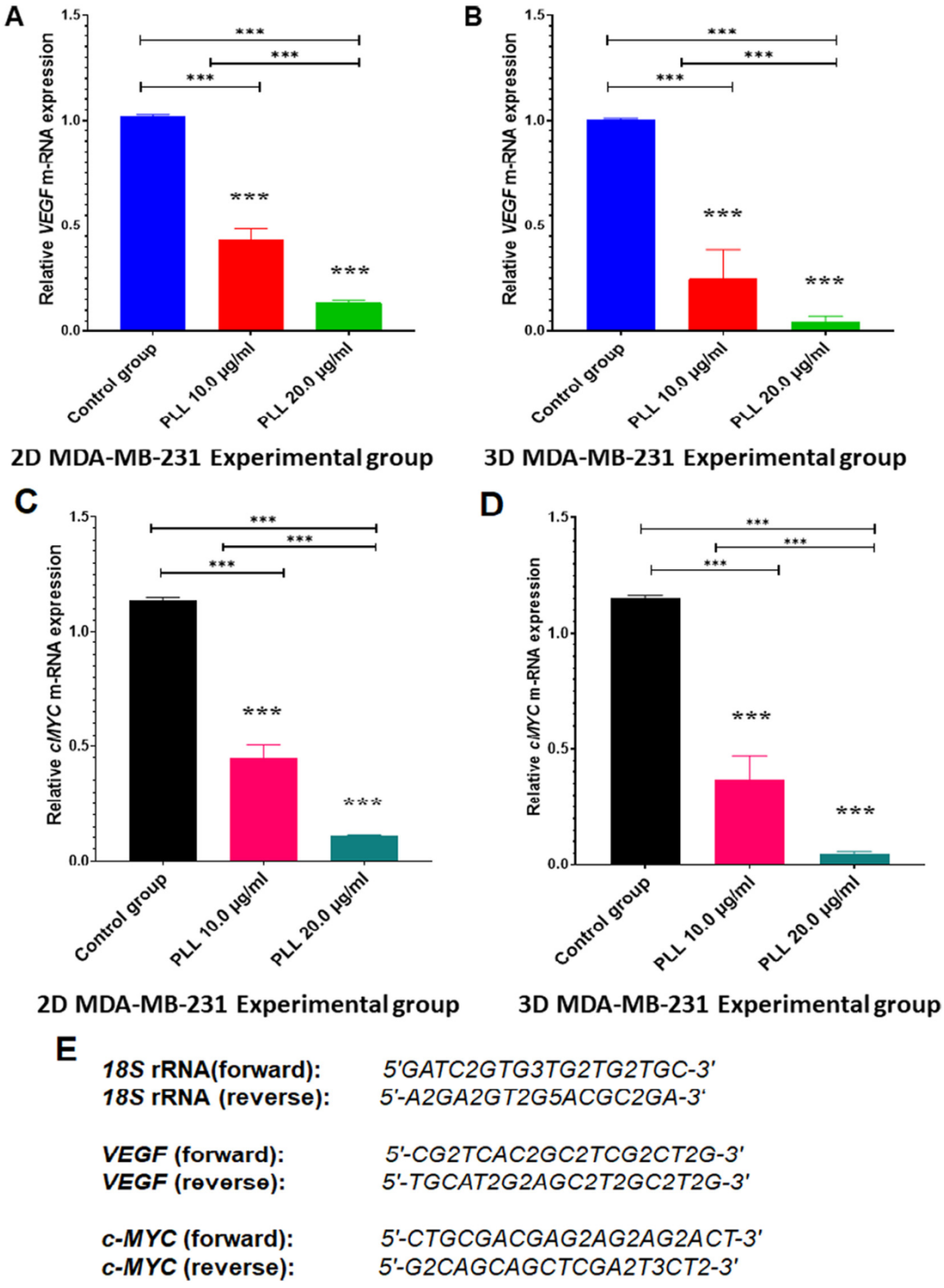

Fig. 5. Suppression of transcription level in MDA-MB-231 aggressive breast cancer cells in both 2D monolayer and 3D tumor microenvironment results in downregulation of tumor-angiogenesis and proliferation markers. (A), (B), (C) and (D) Quantitative real-time polymerase chain reaction (RT-PCR) shows the tumor-angiogenic markers at the mRNA level with significant positive fold decreased in the PLL treated MDA-MB-231 aggressive breast cancer cells compared with the control MDA-MB-231 aggressive tumor cells. Quantitative analysis of transcriptional level shows reduced levels of tumor-neovascularisation and proliferation markers *VEGF* and *c-Myc*. RT-PCR quantitative data are presented as the mean ± SEM of triplicate replicates; $^{***}P < 0.001$.

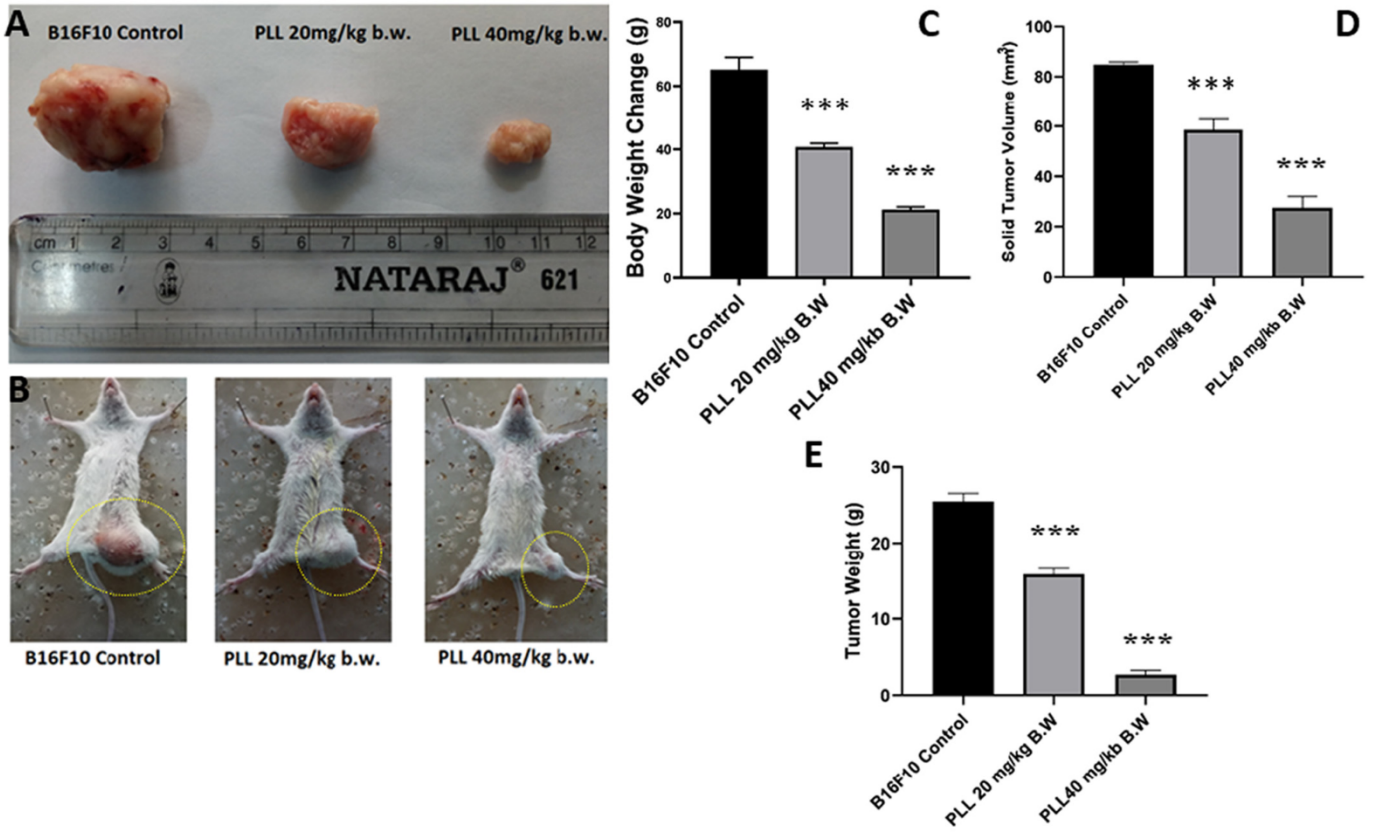

Fig. 6. Effect of PLL treatment on solid B16F10 tumor. (A) 2×10^6 cells/mouse were injected s.c into 5–6-week-old BALB/c mice. (B) After solid tumor grow to ˷100 mm^3, the mice were i.p treated with PLL (20 mg/kg b.w and 40 mg/kg b.w for 21 days. (C), (D) and (E) PLL inhibited the growth of solid tumors. (C) Change the body weight between the drug-treated and control group. (D) and (E) Tumor volume percentage and solid tumors lump in the PLL treated mice significant by smaller than those in the control mice. Data are reported as the mean ± SEM of three different observations (6 animals per treated group). $^{***}P < 0.001$ as compared to B16F10 control group

significantly inhibited by PLL in a concentration-dependent manner ($^{***}P < 0.001$). However, when PLL was applied against PBMC, showed no cytotoxicity and anti-proliferative effect indicating its target specificity.

3.2. PLL inhibits the proliferation of MDA-MB-231 tumor spheroids

We patterned the practicality of the cells in the spheroids after dealing with drugs at diverse concentrations. We experiential that the number of live cells reduced with cumulative drug absorption after 48 h action. The consequences displayed that the reserve charges of PLL to MDA-MB-231 tumor cell spheroids were 91.5%–10.2% respectively as compared to control.

3.3. PLL treatment induces caspase-3 dependent apoptosis in MDA-MB-231 2D and 3D tumor spheroids

To investigate a potential apoptotic effect of PLL on aggressive breast cancer cells, we first addressed the occurrence of apoptosis in 2D and spheroid samples. Consequently, 2D cultures and spheroid segments were immune stained with anti-cleaved caspase-3 antibodies. Next, the information of immune-positive cells remained resolutely the new advanced ImageJ software. As exposed in (Fig. 3), the countenance lights of caspase-3 were virtually high among the 2D and 3D MDA-MB-231 breast cancer cells, wherein caspase-3 appearance was abundantly developed in the 2D-culture than this equal in the 3D-culture. Likewise, besides this, caspase-3 was perceived mostly in the nuclei of 2D-cultured MDA-MB-231 cells in the control group, symptomatic of active caspase-3. Conversely, the quantity of positive apoptotic cells was high in 2D cell culture as a dose-dependent manner compared with the control group. Similarly, apoptotic positive cells were increased significantly in 3D tumor spheroids dose decently after PLL treatment.

3.4. PLL administration suppressed cell predilection in 3D MDA-MB-231 tumor spheroids (Ki67)

To investigate a potential apoptotic effect PLL on aggressive breast cancer cells, we first addressed the occurrence of cell proliferation in 2D and spheroid samples. Therefore, 2D-cultures and spheroid sections

Table 1
Effect of PLL on Tumor weight, Mean Survival Time (MST), Increased Life Span (ILS) and Bodyweight.

	Poly-L-lysine (20 mg/kg b.w)	Poly -L-lysine (40 mg/kg b.w)	B16F10 Control (2×10^6 cells/mouse)
Tumor Weight (gm)	$7.12 \pm 0.01^{***}$	$4.10 \pm 0.05^{***}$	24.29 ± 0.15
% of Tumor Volume	$81.20 \pm 0.07^{***}$	$65.30 \pm 0.06^{***}$	0 ± 0
Tumor growth Inhibition (%)	$24.36 \pm 0.05^{***}$	$30.57 \pm 0.06^{***}$	0 ± 0
MST (days)	$106.16 \pm 0.15^{***}$	$130.08 \pm 0.28^{***}$	$22.35 \pm 0.20^{*}$
% ILS	$76.58 \pm 0.08^{***}$	$98.76 \pm 0.82^{***}$	0 ± 0
Body weight (gm)	$23.61 \pm 0.52^{***}$	$18.50 \pm 0.61^{***}$	$39.02 \pm 0.56^{*}$

Each point represents the mean ± SEM. ($n = 6$ mice per group), $^{*}P < 0.05$, $^{***}P < 0.001$ statistically significant when compared with B16F10 control group.

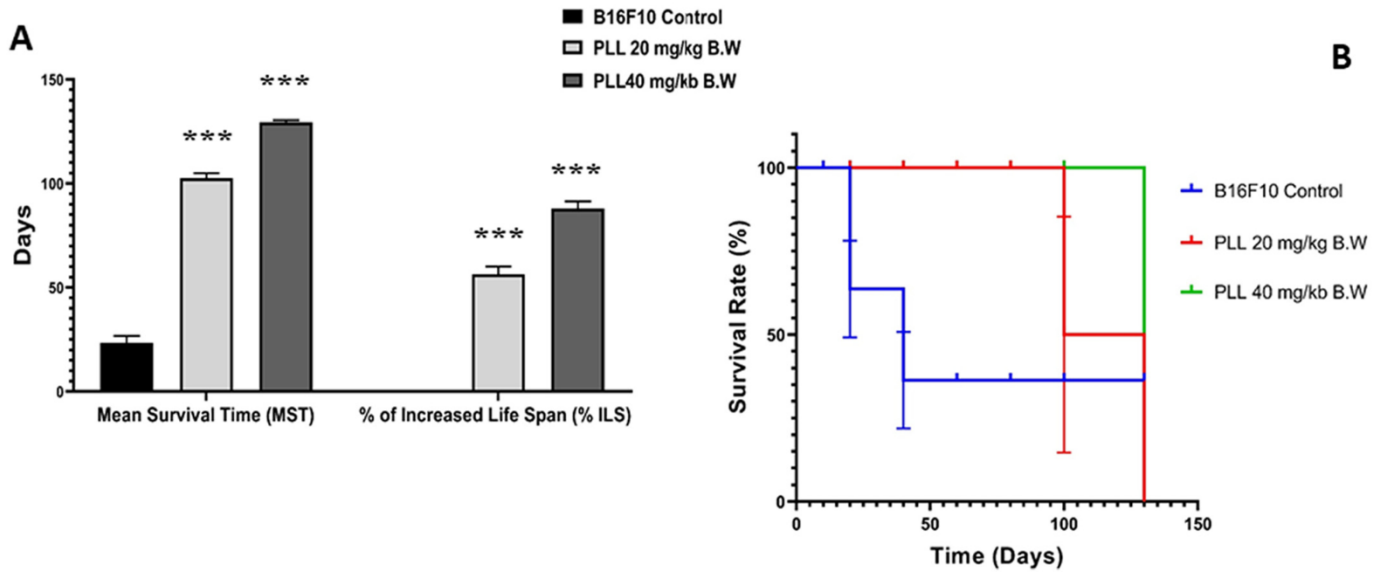

Fig. 7. Effect of PLL treatment on solid B16F10tumor. Effect of PLL on (A) mean survival time (MST) and percentage increase in life span (%ILS). (B)Survival study of synthesized PLL compounds. Effect of PLL on the Kaplan–Meier survival estimate of B16F10-bearing BALB/c mice. Where $n = 6$ for control and PLL treated group.

were immune stained with anti-Ki-67. Subsequently, the numbers of immune-positive cells were determined using the newly developed ImageJ software. This showed fewer proliferating cells in 2D cultures of MDA-MB-231 cells than the control group of MDA-MB-231 cells after PLL treatment. Moreover, the fraction of proliferating positive cells decreased significantly from the control group after PLL treatment.

To explore the relevant effect of PLL on 3D-culture to tumor spheroid, we have shown in (Fig. **4**), the proportion of positive cells for Ki-67 in the 2D and 3D-primary cultured cells significantly decreased respectively after PLL treatment as dose-dependently. These findings confirm that a 3D-primary culture rather than a 2D-primary culture may better indicate like *in-vivo* tumor model in the anti-proliferative feature.

3.5. PLL treatment inhibits the tumor-endogenous angiogenesis and tumor proliferation through the downregulation of VEGF and c-Myc expression

To explore the PLL's influence on the inhibition of tumor-angiogenesis based *VEGF* and *c-Myc* signalling pathway modulation the RT-PCR method was used in MDA-MB-231 aggressive breast cancer cells in both 2D monolayer and 3D tumor microenvironment treated with PLL at the transcript level. We observed that *VEGF* and *c-Myc* mRNA high expression in the aggressive breast cancer cells control group, but the levels were greatly decreased when treated with PLL ($^{***}P < 0.001$) compared with the control group as the dose-dependent manner in both type monolayer 2D and 3D tumor spheroid *in-vitro* tumor model (Fig. 5). According to our study, the PLL treated triple-negative breast cancer cells were significantly inhibited the neovascularization of tumor angiogenesis through the suppression of *VEGF and c-Myc* gene expression level ($^{***}P < 0.001$).

3.6. Acute toxicity assay for drug dose selection in in-vivo assay

For drug dose selection acute toxicity study was done after intoxicating the mice with PLL alone at several doses. Change in the thirst generation and rapid movement were observed at a dose beyond 40 mg/kg b.w. Therefore, for the further study, PLL dose was selected as 20 and 40 mg/kg b.w

3.7. PLL inhibits B16F10 solid tumor growth in BALB/c mice

The average tumor volume in B16F10 control mice increasingly amplified with time up to 69.87 ± 1.25 mm^3 from 12.35 ± 4.20 mm^3 (at day 1st) for 21 days post-tumor imbedding study. In PLL drug-induced groups the percentage of tumor volume was pragmatic in respect to the control group are 81.20 ± 0.07 for 20 mg/kg b.w and 65.30 ± 0.06 for 40 mg/kgb.w. This designates tumor volume decreases dose-vulnerably (Fig. 6) and (Table 1). In addition, PLL treatment significantly condensed tumor weight associated with B16F10 bearing control group ($^{***}P < 0.001$) mice (Fig. 6). The body weight vicissitudes were knowingly developed in PLL preserved groups compared to control representing the consequence of PLL in averting the tumor development (Fig. 6) and (Table 1).

Table 2
Effect of PLL on haematological parameters in B16F10 bearing BALB/c mice.

	Poly-L-lysine 20 mg/kg b.w	Poly-L-lysine 40 mg/kg b.w	B16F10 Control (2×10^6 cells/mouse)	Normal BALB/c Mice
Haemoglobin (gm %)	$8.39 \pm 0.01^{**}$	$11.59 \pm 0.01^{**}$	$5.20 \pm 0.15^{**}$	12.6 ± 0.14
Erythrocyte (RBC) (cells x $10^6/mm^3$)	$6.86 \pm 0.02^{**}$	$8.60 \pm 0.01^{**}$	$3.02 \pm 0.01^{**}$	9.59 ± 0.02
Leucocytes (WBC) (cells x $10^6/mm^3$)	$8.26 \pm 0.03^{**}$	$12.03 \pm 0.02^{**}$	$24.17 \pm 0.03^{**}$	13.4 ± 0.01
Neutrophil (%)	$31.10 \pm 21.90^{*}$	$30.17 \pm 0.03^{**}$	$74.11 \pm 0.03^{**}$	30.08 ± 0.06
Lymphocyte (%)	$46.78 \pm 0.01^{**}$	$61.34 \pm 0.02^{*}$	$27.06 \pm 0.05^{**}$	68.32 ± 0.25
Monocyte (%)	$1.76 \pm 0.02^{*}$	$2.38 \pm 0.03^{*}$	$1.10 \pm 0.01^{*}$	2.15 ± 0.03

Each point represents the mean ± SEM. ($n = 6$ mice per group), $^{**}P < 0.01$ and $^{*}P < 0.05$ statistically significant when compared with the normal saline group and B16F10 control group.

Table 3
Effect of PLL on serum biochemical in B16F10 bearing BALB/c mice.

	Poly-L-lysine 20 mg/kg b.w	Poly-L-lysine 40 mg/kg b.w	B16F10 Control (2×10^6 cells/mouse)	Normal BALB/c Mice
Bilirubin Total & Direct: (mg/dl)	$0.31 \pm 0.01^{**}$	$0.26 \pm 0.02^{**}$	$0.37 \pm 0.01^{**}$	0.42 ± 0.02
Serum Protein (Total) (mg/dl)	$6.28 \pm 0.08^{**}$	$6.62 \pm 0.08^{**}$	$2.34 \pm 0.11^{**}$	6.82 ± 0.08
AST(SGOT) (IU/l)	$56.24 \pm 0.01^{**}$	$37.1 \pm 0.02^{**}$	$79.04 \pm 0.05^{**}$	38.19 ± 0.03
ALT (SGPT) (IU/l)	$42.10 \pm 0.02^{**}$	$30.04 \pm 0.02^{**}$	$66.28 \pm 0.03^{**}$	28.35 ± 0.03
Serum Alkaline Phosphates (IU/l)	$90.02 \pm 0.03^{**}$	$78.16 \pm 0.02^{**}$	$124.25 \pm 0.03^{**}$	77.28 ± 0.01
Creatinine (mg/dl)	$0.76 \pm 0.01^{*}$	$0.8 \pm 0.02^{*}$	$0.62 \pm 0.02^{*}$	0.82 ± 0.02

Each point represents the mean ± SEM. ($n = 6$ mice per group), $^{**}P < 0.01$ and $^{*}P < 0.05$ statistically significant when compared with the normal saline group and B16F10 control group.

3.8. PLL enhance the survival of B16F10 bearing BALB/c mice

The survival of PLL treated B16F10 bearing mice significantly increased as compared to B16F10 bearing control group. The %ILS increases in PLL at 20 and 40 mg/kg b.w. was found to be in a dose-dependent manner (Table 1) and (Fig. 7).

3.9. Effect of PLL on haematological parameters

Haematological limits of PLL preserved and untreated (21 days) tumor-bearing mice were assessed (Table 2). Haemoglobin and RBC level that reduce usually throughout the development of the tumor was originated to advance in mice preserved with PLL, PLL conduct reduced WBC amount compared with the B16F10 control. In the discrepancy count of WBC, lymphocytes and monocytes reduced and neutrophils augmented in the B16F10 control group when associated with healthy controls. PLL pickled at diverse doses as above significantly vicissitudes the applicable limitations approximately, to the normal values (Table 2).

3.10. Effect of PLL on biochemical parameters

(Table 3) confirmed that the biochemical strictures like SGOT, SGPT, SALP, and bilirubin knowingly diminished in a dose-in need of manner (20 and 40 mg/kg b.w.) as associated with the B16F10 control group. Consequences also demonstrate that total protein gratified augmented dose-dependently.

3.11. Histopathology of liver and kidney tissue

To inspect the possible character of PLL in tissue-precise metastasis in melanoma models, the xenograft melanoma tumors as shown in (Fig. 8), were ventrally dismembered and metastatic lesions such as liver and kidney were unglued and analysed by histopathologically (Fig. 8). The data designated that tumors aggregated by control cell metastasis in the liver and kidney, however, PLL melodramatically repressed this metastasis (Fig. 8) representative that PLL constrains melanoma growth, angiogenesis, and metastasis in subcutaneous BALB/c mice models. The data recommended the noteworthy melanoma metastasis properties in the liver and kidney of control B16F10 inoculated mice (Fig. 8). Furthermore, we have noticed numerous metastatic foci in the tissue sections of the liver and kidney of control B16F10 inoculated BALB/c mice by histopathology with H&E staining. In total, the data on the condition indicates that overexpression of PLL meaningfully decreases melanoma metastasis to the liver and kidney in the murine melanoma model. H & E stained sections of liver slices of PLL test drug-treated mice, shown in (Fig. 8), exhibiting the presence of all the normal features, including circular hepatic portal vein and branch of the hepatic artery, as marked by arrows. The hepatocytes show prominent nuclei (Fig. 8) and the tissue section comprises hepatic sinusoids as usual. On the contrary, for the B16F10 control mice (Fig. 8), none of the regular features as abovementioned could be found, rather, it reveals extensive hepatocellular lesions, as shown in subpanel (ii), as pyknotic nuclei (marked by arrow), exhibiting necrotic hepatocytes. On treatment using the test drug, PLL at a dosage of 20 mg/kg b.w, very fewer amounts of phenotypic alteration and altered hepatocyte population

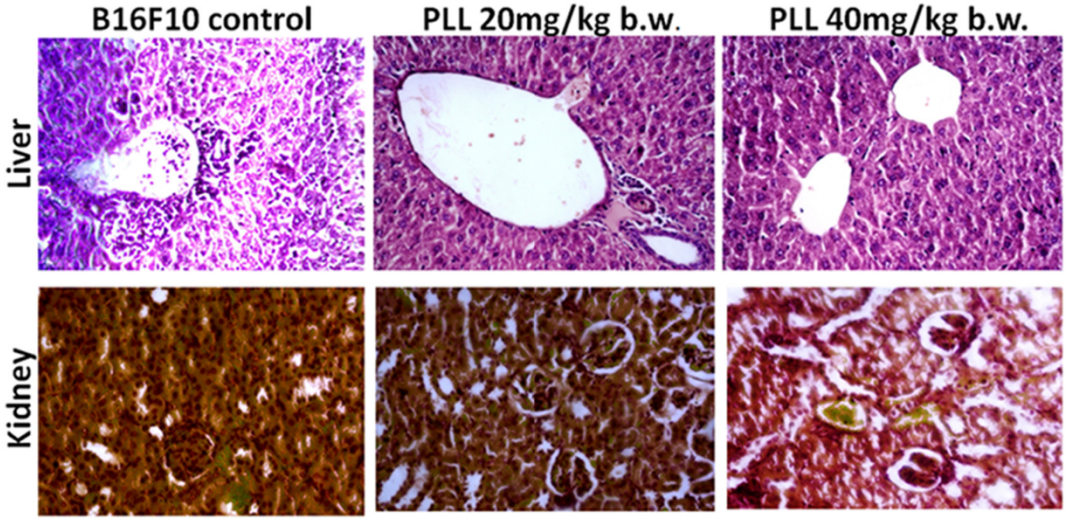

Fig. 8. H&E staining of livers and kidneys from PLL treated group and control group BALB/c mice. *In-vivo* histopathological analyses of B16F10 tumor-inducedBALB/c mice liver and kidney after treatment with PLL for 21 days. H&E staining images of liver and kidney sections of PLL treated mice demonstrating inflammatory cells infiltration inBALB/c mice sections. $n = 3$ mice per group. Scale bar = 100μm. Magnification: 200×.

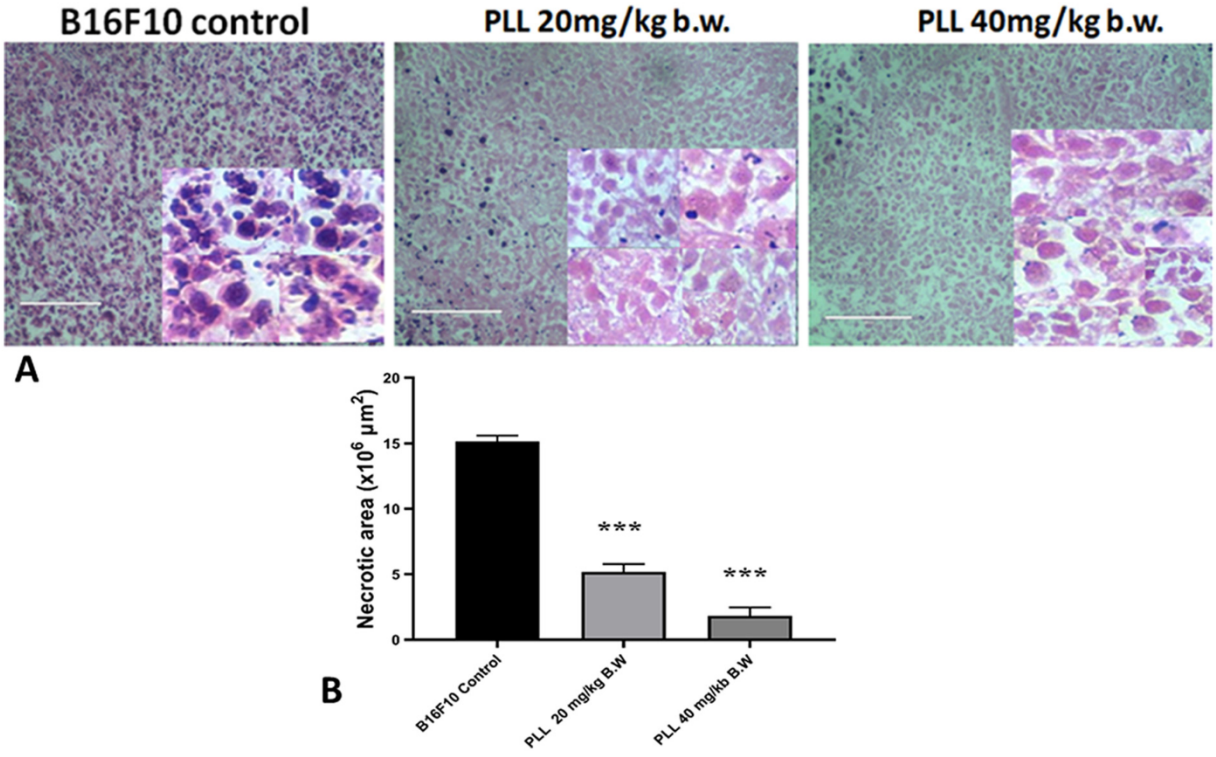

Fig. 9. *In-vivo* histopathological analyses of B16F10 tumor. (A)Histopathological examination of B16F10 solid tumor. We have shown untreated B16F10-bearing mice tumor section infiltration of subcutaneous tissue with tumor cells, newly formed blood capillaries; and leukocyte infiltration, B16F10 tumor-bearing mice treated with PLL 20 mg/kg have shown extensive cell death; fibrosis; skeletal muscles; destructed blood vessels, haemorrhage; extensive infiltration of the subcutaneous tissue with tumor cells; tumor cells with anisocytosis, B16F10 tumor-bearing mice treated with PLL 40 mg/kg have shown moderate infiltration of the tumor cells; numerous leukocyte infiltration; huge numbers of tumor cells infiltrating the skeletal muscles; less infiltration with tumor cells; extensive necrosis and fibrosis; islets of viable tumor cells; extensive necrosis. Tissue sections were stained with H&E dyes (scale bar = 100μM). (B) The quote of the percentage of necrotic area in sections of tumors harvested on d 22post-treatment. In each section per tumor four random areas were counted and three tumors were harvested in each treatment group. The quota of the percentage of necrosis was determined using ImageJ software. Mean ± SEM, $n = 3$.

were found marked by the presence of healthy hepatocytes although a mild dilation of the central vein could be observed. On escalation of the dose to 40 mg/kg b.w, (Fig. 8) the cellular and overall features were close to normal mice liver histopathology, marked by the presence of healthy hepatocytes, regular central vein, branch of the bile duct, and hepatic artery, deformity in the hepatic artery and irregular bile duct could also be found.

Furthermore, the kidneys of mice treated with PLL did not show any changes, but a slight lymphocytic infiltrate was observed in the kidneys of BALB/c mice treated with PLL 40 mg/kg b.w. As shown in (Fig. 8) histological examination of the kidney indicated normal glomeruli and renal tubules in all mice groups except the B16F10 control group. (Fig. 8). In kidney histology of the PLL drug-treated mice exhibited an almost normal architecture structure as found compare with the B16F10 control group.

3.12. Effect of PLL on histopathological changes of solid B16F10 tumor

The histological inspection was done complete H&E staining of tumor sections. Our consequences designate that tumor tissue subsequent from B16F10 control mice has a chaotic preparation of cancer cells and a high cell density. The cells were voided or round and presented a high nucleus which was indistinctly stained with clear signs of heteromorphism and hyperplasia. Also, it displayed complete anaplastic cancer cells with zones of necrosis and focal hemorrhagesh immering the practicality and aggressiveness of the tumor invading cellular infiltration, cords of malignant cells and large tumor cells among muscle fibres, high mitotic movement in B16F10 bearing mice. As revealed in (Fig. 9) and (Table 4) the number of tumor cells in the PLL treated groups reduced noticeably by cells that were polygonal and light stained. Also, tumor cell nuclei shapes were uneven, and the shallow of the nucleic membrane was rough. The nucleus was broken, less tumor invasion and cellular infiltrates, modest mitotic movement and evidently amplified apoptotic bodies. The mice of the PLL treated groups showed lesser necrotic areas and decrease the quantity of mitotic figures.

3.13. Changes in the morphology of B16F10 tumor tissue cells after PLL treatment

The inhibitory effect of PLL on B16F10 cells of the mice model was pragmatic by Giemsa staining. The test groups resemble Giemsa staining

Table 4
Effect of PLL on the histopathological changes in solid tumor (B16F10) bearing BALB/c Mice ($n = 3$).

Group	Tumor Infiltration at Margin	Inflammatory cells Infiltration at Edge	Mitotic Index (no of MFs in 12 HPFs)	Apoptotic index (no of Abs in HPFs)
B16F10 control	+++	+++	26	3
PLL (20 mg/kg b.w)	++	++	5	9
PLL (40 mg/kg b.w)	+	+	3	18

Tumor sections from three different tumors in each group, and four randomly selected areas from each tumor were analysed (12 HPFs); MF = Mitotic figure; HPF = High power field (X400); Abs = Apoptotic body; (+), mild; (++), moderate; (+++), sever.

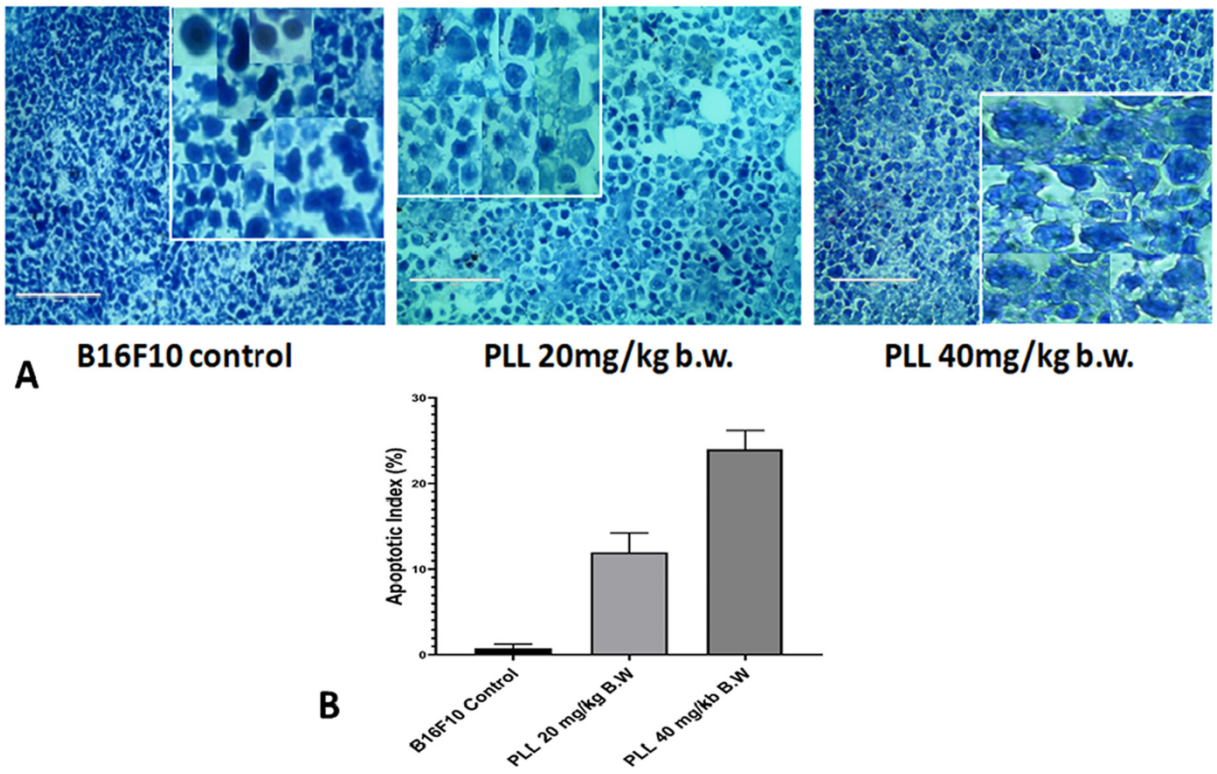

Fig. 10. Histopathology of the B16F10 tumor mass stained with Giemsa staining. (A) Morphological changes occurred after treatment PLL. Giemsa staining has shown the characteristic features of apoptosis, including the reduction of cell size, condensation and aggregation of nuclear chromatin, and nuclear fractionation, cellular blebbing, were observed in PLL treated B16F10 tumor section as dose-dependently. (B) The quote of the percentage of apoptotic index in sections of tumors harvested on d 22 post-treatment. In each section per tumor four random areas were counted and three tumors were harvested in each treatment group. The quota of the percentage of the apoptotic index was determined using ImageJ software. Mean ± SEM, $n = 3$.

that validates blebbing of the plasma membrane (marked by arrow), shown, whereas, the formation of apoptotic bodies could also be observed in (Fig. 10). In general, the control B16F10 cells have good morphology with intact plasma membrane whereas, in the case of the test PLL drug, the apoptotic bodies and the nuclear condensation is apparent (Fig. 10). In the PLL drug-pickled group for Group II that receives 20 mg/kgb.w. of PLL, chromatin condensation, blebbing of the plasma membrane, irregularity in cell morphology, was observed in (Fig. 10). As the dose of PLL is intensified to twice the former, i.e., 40 mg/kg b.w. in case if Group III mice, displayed in both the phenomenon of cellular blebbing, followed by cell shrinkage, cytoplasmic irregularity, nuclear fragmentation irregular shape, and formation of the apoptotic body as a dose-dependent manner (Table 5).

3.14. PLL promotes apoptosis of B16F10 solid tumor tissues

The flow cytometry was displayed to inspect the apoptosis percentage. Annexin V-FITC discolouration and PI accumulation were used to determine the percentage of apoptotic cells. Prematureproceedings in the apoptotic process is the loss of plasma membrane asymmetry, accompanied by translocation of phosphatidyl-serine (PS) from the inner to the outer membrane leaflet, thereby exposing PS to the external environment [25]. Annexin-V single-positive cells (annexin+/PI-) were measured as early apoptotic, double-positive cells (annexin+/PI+) as of late apoptotic, whereas double-negative cells (annexin-/PI-) and PI single-positive cells (annexin-/PI+) on behalf of non-apoptotic and necrotic cells, correspondingly. The phospholipid-binding protein annexin V has a high sympathy for PS and predicaments to cells fluorescently labelled with FITC (fluorescein isothiocyanate). The percentages of apoptosis, as strong-minded by annexin V-FITC/PI flow cytometry study, are revealed in (Fig. **11**). PLL conduct groups (20 and 40 mg/kg b.w presented significant upsurges in apoptosis compared with the control group($^{***}P < 0.001$).

3.15. PLL potentiated the apoptotic effect on B16F10 solid tumor in-vivo BALB/c mice model

Western blot assays (Fig. 12) showed that there was an increase in cytochrome-*c* after PLL treatment 20 and 40 mg/kg b.w respectively as a dose-dependent manner. The increased cytosolic cytochrome-*c* ultimately activate caspase-9 which in turn activates caspase-3 and activated PARP cleavage [26] (Fig. 12) leading to induction of apoptotic signalling pathway causing the B16F10 tumor cell death due to

Table 5
Apoptotic effect of PLL on the histopathological changes in solid tumor section (B16F10) bearing BALB/c Mice ($n = 3$).

Group	Inflammatory cells Infiltration at Edge	Mitotic Index (no of MFs in 12 HPFs)	Apoptotic index (no of Abs in HPFs)
B16F10 control	+++	29	1
PLL (20 mg/kg b.w)	+	7	12
PLL (40 mg/kg b.w)	+	2	30

Tumor sections from three different tumors in each group, and four randomly selected areas from each tumor were analysed (12 HPFs); MF = Mitotic figure; HPF = High power field (X400); Abs = Apoptotic body; (+), moderate; (+++), sever.

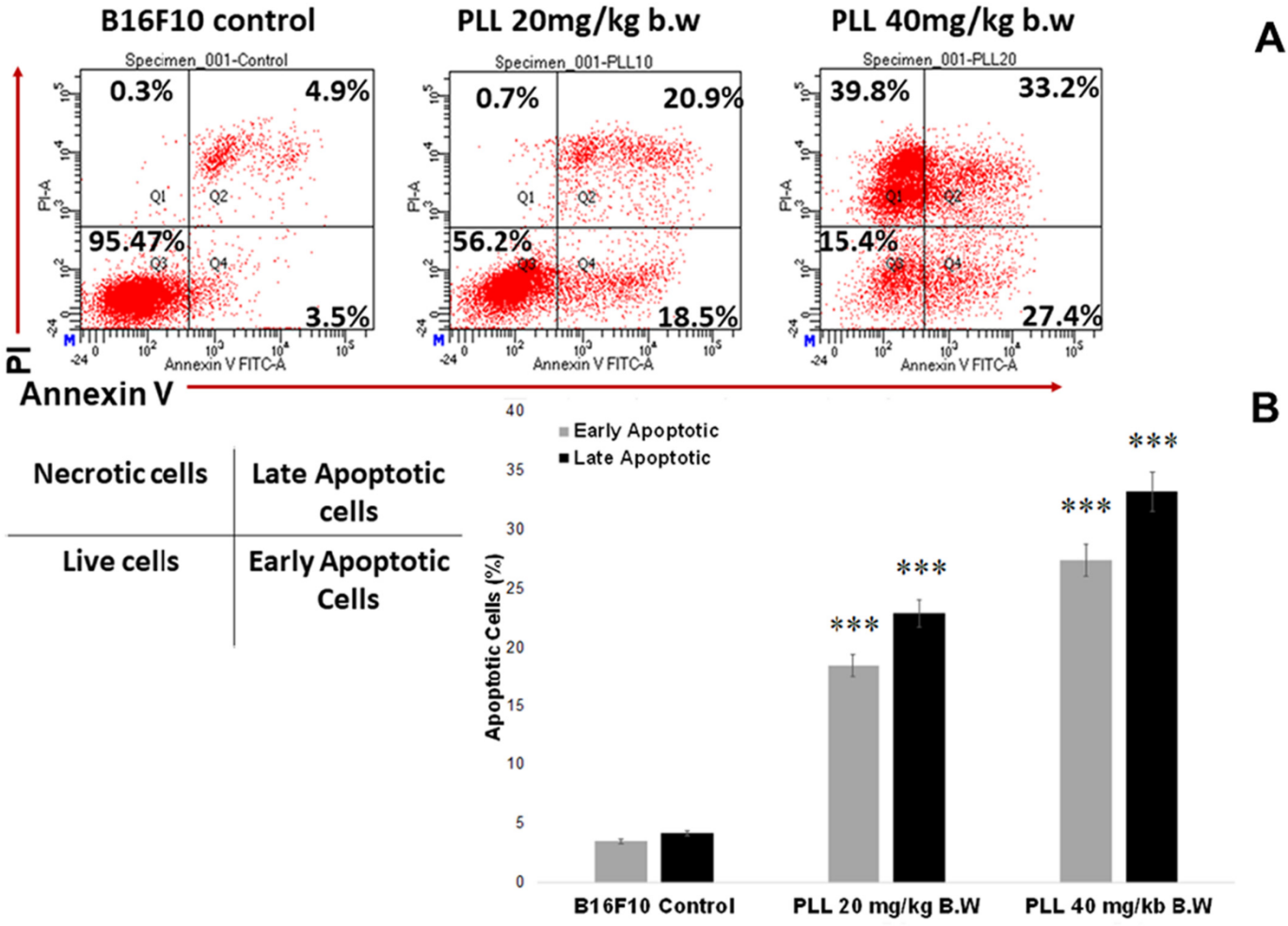

Fig. 11. PLL induced B16F10 cell apoptosis. (A) Representative flow cytometry apoptosis level analysis by data from Annexin V-FITC/ PI staining. A representative flow cytometric analysis of apoptosis in B16F10 cells is shown. The fluorescence intensity of annexin V/FITC is plotted on the x-axis, and PI is plotted on the y-axis. FITC−/PI−, FITC+/PI−, FITC+/PI+, FITC−/PI+ was regarded as living, early apoptotic, late apoptotic and necrotic cells, respectively. (B) Quantitative results of cell apoptosis determined using Annexin V-FITC/PI flow cytometry analysis and expressed as the mean ± SEM of three experiments. $^{***}P < 0.001$ *vs.* control group.

increased proteolytic activity within the *in-vivo* B16F10 cells. This phenomenon indicates our results suggest that PLL at 20 and 40 mg/kg b. w. activates the mitochondrial intrinsic pathway of apoptosis to induce cytotoxicity in B16F10 tumor cells.

3.16. PLL inhibits tumor-induced neovascularization in B16F10 solid tumor

CD34 is one of the maximum used endothelial cell indicators accustomed to highpoint tumor blood vessels. It is an external glycoprotein that places of interest perivascular stromal cells. CD34 examination displayed plentiful great blood vessels in B16F10 control tumor. PLL repressed CD34 countenance in B16F10 solid tumor (Table 6; Fig. 13). CD34 has been used as a marker for micro vessel density (MVD) approximation and MVD morals have been associated among the numerous groups. As apparent from (Fig. 13) PLL (20 mg and 40 mg/kgb.w.) diminished the % MVD as associated to control BALB/c mice in a dose-dependent manner, representing potent anti-angiogenic action of the PLL.

In (Fig. 14), additional, to authenticate this consequence, I had completed western blot to study an angiogenesis marker. VEGF and VEGFR2 are important angiogenesis growth factors. This consequence designates that in the B16F10 solid tumor PLL preserved mice, a significant down-regulation of VEGF and VEGFR2 level as the dose-dependent manner was experimental when associated to the VEGF and VEGFR2 level from B16F10 control group mice.

3.17. PLL administration suppresses cell proliferation in in-vivo B16F10 solid tumor

Subsequently, lessons have been completed on PLL interceded destruction the B16F10 persuaded solid tumor development was escorted by a reserve of cell proliferation initiation in tumor tissues. As pragmatic in (Fig. 15), control B16F10 tumor segments exposed robust nuclear Ki-67 expression intimating at sensitive cell propagation. In dissimilarity, PLL management occasioned in an important reduction of Ki-67 positive cells and proliferation index (Fig. 15); (Table 7). This consequence designated that PLL direction reserved subcutaneous B16F10 solid tumor development *in-vivo* by dropping cell proliferation and plummeting tumor angiogenesis.

3.18. VEGF and c-Myc expression in tumor-suppressing endogenous angiogenesis and proliferation inhibition (VEGF, c-Myc)

To explore the PLL's influence on the *VEGF* and c-*Myc* signalling pathway, the RT-PCR method was used to study the effects on the expression of *VEGF* and *c-Myc* mRNA in B16F10 tumor cells when treated with PLL. In B16F10 tumor cells, RT-PCR was performed to investigate whether the inhibition of *VEGF* and *c-Myc* levels occurred due to alterations at the transcript level. We observed that *VEGF* and *c-Myc* mRNA high expression in B16F10 tumor cells, but the

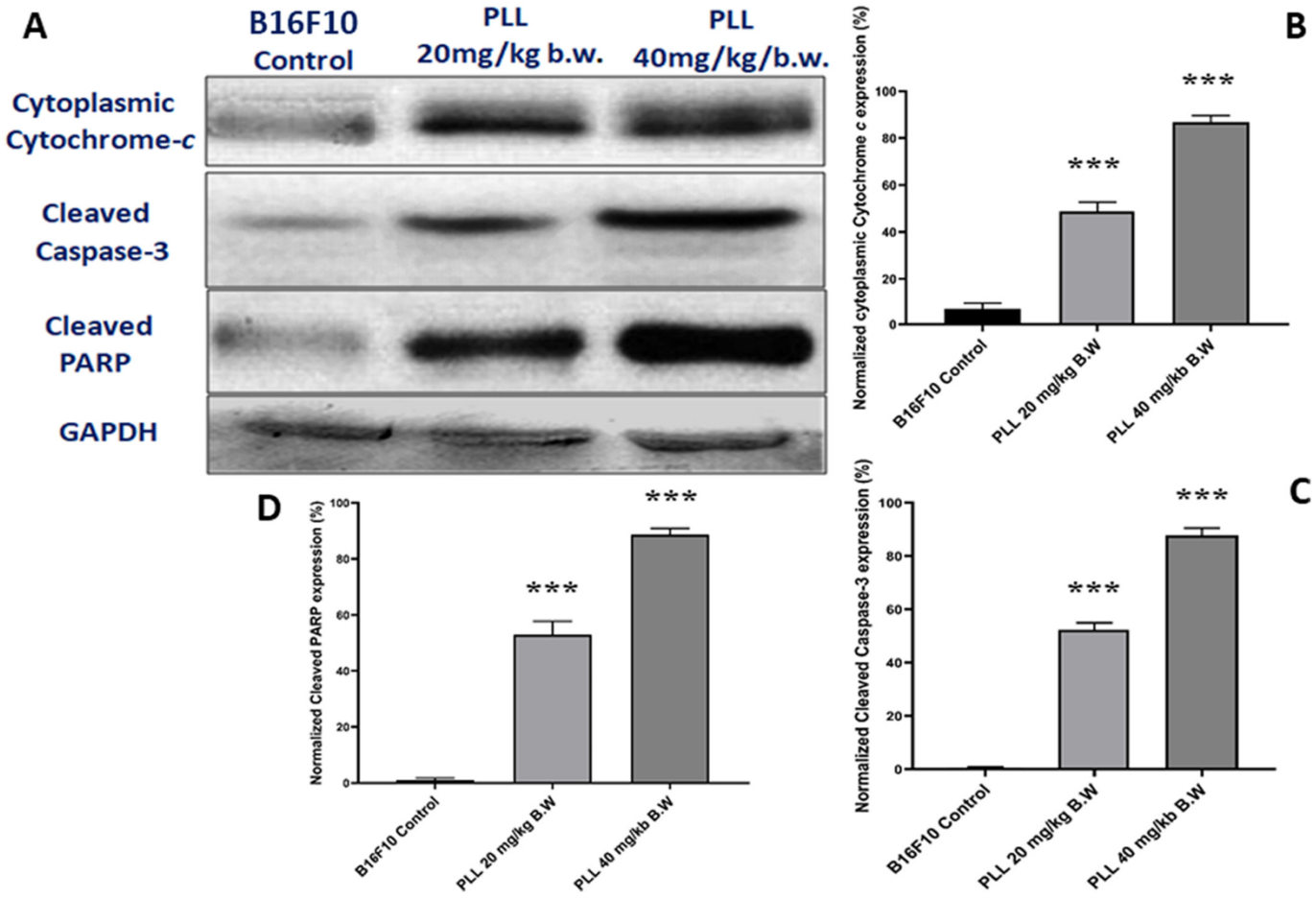

Fig. 12. Apoptosis detection in *in-vivo* B16F10 murine melanoma cells induced by PLL, western blot analysis. Quantitation of significant dose-dependent increase in cytochrome *c*, cleaved caspase 3, and cleaved PARP activity upon PLL treatment with 20 and 40 mg/kg b.w.(A) Tumor lysates were harvested and the apoptotic proteins (cytochrome *c*, caspase 3, and PARP) were detected by western blotting. (B, C, D) The relative amounts of cytochrome *c*, cleaved caspase 3 and cleaved PARP *versus* GAPDH were determined by western blotting results and ImageJ densitometric analysis.

levels were greatly decreased when treated with PLL ($^{***}P < 0.001$) compared with the control group (Fig. **16**). The increase in inhibition, as compared with the control group, was statistically significant in the B16F10 tumor cells that were treated with 20 and 40 mg/kg b. w PLL ($^{***}P < 0.001$).

3.19. PLL inhibited angiogenesis in the CAM model

We also appraised the *in-vivo* anti-angiogenic motion of PLL by the CAM assay. As demonstrated in (Fig. 17), conduct with PLL for 48 h instigated a dose-dependent lessening in the branching of new capillaries from the departing blood basal vessels associated with the control group. The quantitative investigation exposed that PLL in quantities of 10, 20 and 30 μg/ml abridged blood vessels by 26.8%, 47.2%, and 77.3%, correspondingly. These consequences recommend that PLL inhibited angiogenesis *in-vivo* condition.

Table 6
Semi-quantitative analysis of immunohistochemical staining of CD34 in tumor tissues for the molecular marker ($n = 3$).

Group	CD-34
B16F10 control	+++
PLL (20 mg/kg b.w)	++
PLL (40 mg/kg b.w)	+

+ (Weak Staining); ++ (Moderate staining); +++ (Strong Staining).

4. Discussion

Cancer is characterized by uncontrolled cell proliferation and a reduction in cell apoptosis [27]. In case of such a disease, cells in the human body grow within an organized 3D matrix, and the behaviour of each cell is controlled *via* their interactions with their immediate neighbours and with the extracellular matrix [19,28]. The growth and maintenance of any normal tissue depend on cellular interactions, and the physiological fate of these tissues is subject to the 3D environment, which includes a variety of growth factors, hormones, and adhesion molecules, as well as a complex extracellular molecular matrix. Cells under 3D culture conditions have been determined to sustain and divide rapidly, and evidence a characteristically asymmetrical shape as compared with that of cells in living tissue [18]. Moreover, for breast cancer, 3D culture conditions provide an important model system to understand the mechanism of the regulation of cancer cell proliferation and also to assess of different anticancer drugs [29]. Aggressive breast cancer induces a strong fibro-proliferative response with the synthesis of type-I collagen by which the metastatic nature of breast cancer is being achieved [18]. Therefore, in this study, we utilized a collagen-based 3D culture method for our investigation, and we could originally observe more evident pro-apoptotic effects of PLL in the 3D-cultured MDA-MB-231 cells. With PLL treatment, it was confirmed that PLL downregulated the proliferation and induced apoptotic effect slightly better in 3D cultured MDA-MB-231 cells as compared with the 2D culture. This suggests the capability of PLL in modulating the tumor microenvironment that leads to its potential efficacy in an *in-vivo* condition

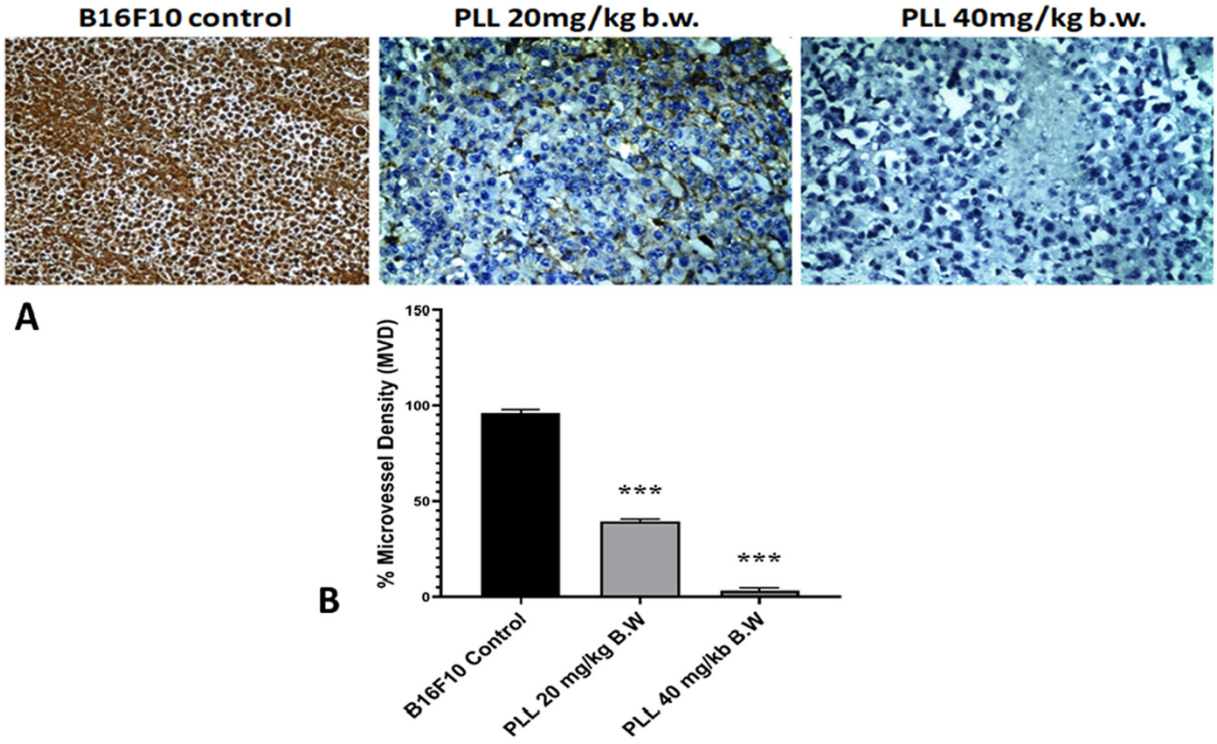

Fig. 13. Treatment with PLL inhibits tumor angiogenesis in BALB/c mice model of B16F10 tumor through down-regulation of CD34 in tumor cells. (A) Immuno-staining and micro vessel density of CD34 expression in B16F10 tumor-induced BALB/c mice after treated with PLL exhibiting the reduction of neovascularization dose-dependently. (B) Immunohistochemical staining for CD34 was examined in BALB/c mice models of B16F10 tumor cell with or without PLLtreatment. The image was captured at 200× magnification. Micro vessel density (MVD) was counted under the microscope at 200× magnification and 25 fields from each group were counted. Each bar represents the mean ± SEM, $n = 3$ tumors. $^{***}P < 0.001$ as compared to control group mice.

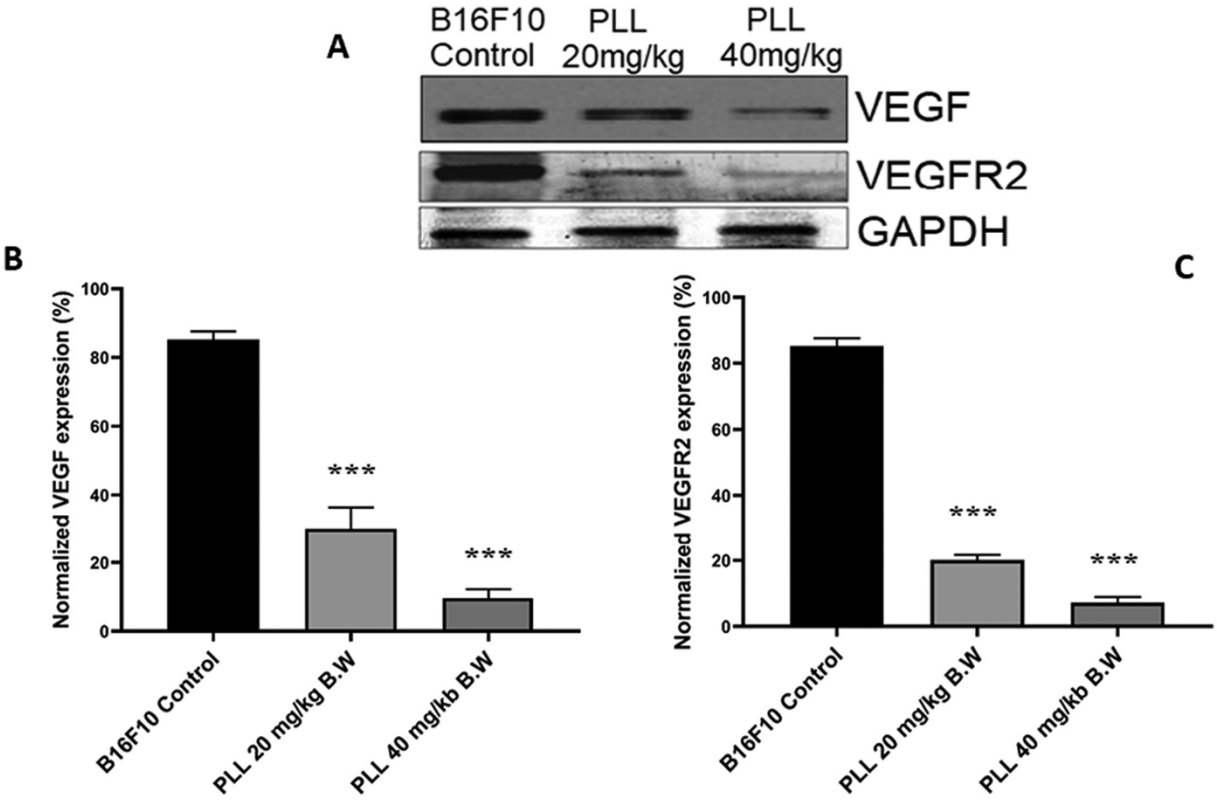

Fig. 14. Differential tumor angiogenesis protein expression of VEGF and VEGFR2 in B16F10 tumor cells. (A) Expression VEGF and VEGFR2, protein was analysed by western blot in B16F10 tumor cells. (B, C) Densitometric analysis showing down-regulation of VEGF and VEGFR2 protein expression. Each value represents the mean ± SEM of three independent experiments, each performed in triplicate $^{***}P < 0.001$ as compared to control group mice.

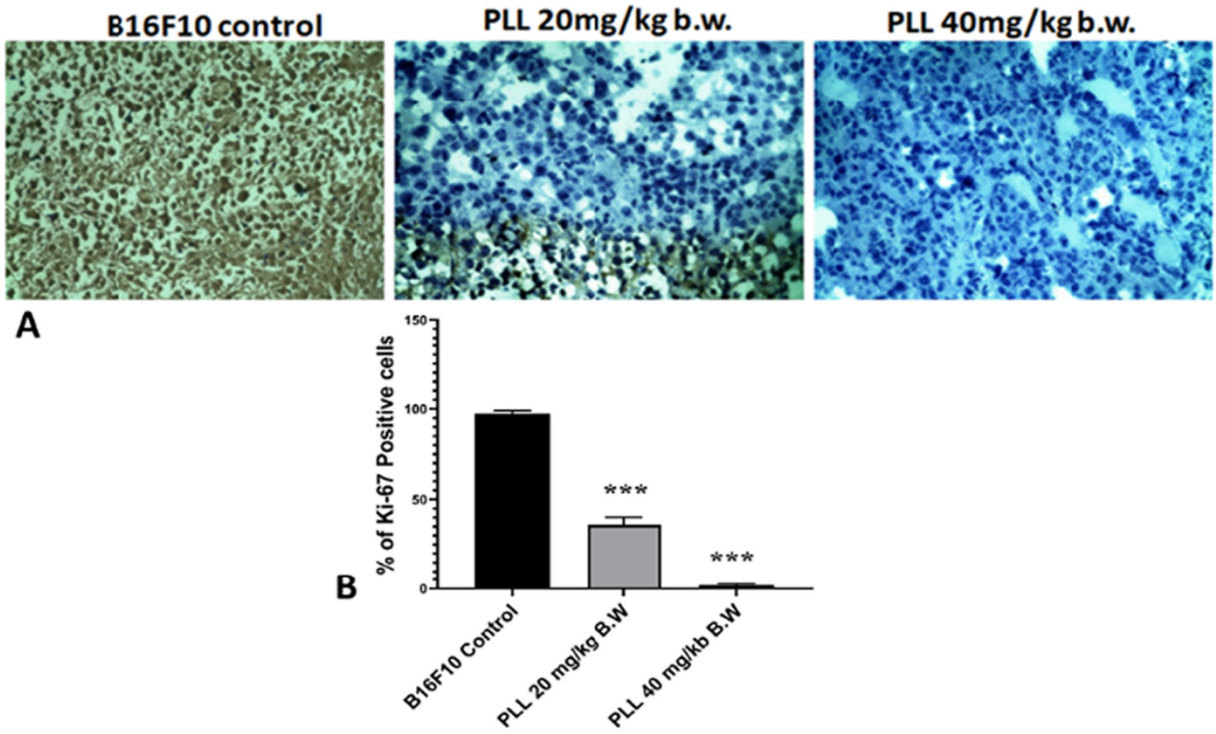

Fig. 15. Ki-67 expression by immunohistochemistry in B16F10 induced BALB/c tumor model. PLL suppresses tumor growth in the BALB/c mouse model. (A) Comparison of cell proliferation by immunohistochemical analysis using the Ki-67 marker in tumor cells derived from PLL treated B16F10 tumor and control B16F10 tumor tissue sections. PLL administration reduced Ki-67 positive cell populations in DAL solid tumors compared with the control group. The intensity of Ki67-positive cells was calculated with ImageJ software (×400). (B) Quantification of Ki-67 index (% of positive cells). The average percentage of Ki-67 positive cells in tumors arising from PLL treated groups was significantly reduced than those in the control group. Each bar represents the mean ± SEM, $n = 3$ tumors. $^{***}P < 0.001$ as compared to the control group of mice.

also. As the 3D culture mimics the tumor microenvironment, therefore, these results fascinated us to investigate the activity of PLL against the B16F10 induced BALB/c mice tumor model.

PLL dose was selected on which acute toxicity does not appear in the mice's body. B16F10 induced tumor cells which were treated with PLL was perfused. It exerted morphological alteration that indicates a possible death by apoptosis because they have shown cytoplasmic contraction, and nuclear fragmentation [14,15,30].

Studies have shown that PLL exerted its cytotoxic properties through apoptosis. Our results showed that the PLL induced cellular apoptosis because we observed an increase in Annexin-V and PI-positive cells, DNA fragmentation, and activation of caspase-3 and cleaved PARP in cells treated with this test drug against B16F10 induced cancer cells in mice. The *in-vivo* results are promising because PLL in a dose-dependent manner caused a reduction in tumor mass in a melanoma murine model, proving the anti-proliferative and antitumor effects of PLL. Thus, PLL could induce mitochondrial-mediated apoptosis by regulating Bcl-2 family members and the activation of PARP in melanoma B16F10 cells.

Table 7
Ki-67 proliferation index (PI) determination.

Group	Ki-67 index (%)
B16F10 control	48.0 ± 5.7
PLL 20 mg/kg b.w	16.5 ± 6.1***
PLL 40 mg/kg b.w	4.8 ± 2.1***

Statistically significant changes as a compound with tumor control group (***$P < 0.001$).

In the present study, the western blot data for cytochrome-*c* showed a significant increase of this protein in the cytosol of PLL treated B16F10 tumor cells as compared with the untreated control group. Thus, suggesting that mitochondrial release of cytochrome-*c* was triggered by the test drug PLL. Increasing levels of pro-apoptotic proteins such as Bax, while decreasing levels of the anti-apoptotic protein, for instance, Bcl-2 by PLL was also observed in PLL treated mice. Besides this, PLL also upregulates the activation of Caspase-3 and cleaved PARP in B16F10 tumor cells of intoxicated BALB/c mice. The imbalance meant between Bax/Bcl-2 might create a trickling effect which then ultimately leads to the activation of caspase-3 and they will leave many important cellular substrates including PARP and finally causing cell death by apoptosis [31,32].

Besides this Ki67, which is a proliferation marker was also found to be downregulated after PLL administration. This study also elucidated that PLL treatment further suppressed the expression of downstream genes, such as c-Myc, in the *in-vivo* B16F10 mice model. Thus, down-regulation of the levels of proliferative c-Myc protein products is likely linked with PLL's ability to induce apoptosis, proliferation inhibition, and neovascularization inhibition in tumor cells. Myc proto-oncogene is a prominent driver in the development of malignant metastatic tumors [33,34]. Our findings reveal that PLL targets the c-Myc pathway that can regulate the production of VEGF and angiogenesis. c-Myc a proto-oncogene is believed to be one of the candidate oncogenes that can induce the expression of angiogenesis [35,36]. Our findings revealed that PLL treatment targets the c-Myc pathway that can regulate the production of VEGF and angiogenesis. Therefore, it is hypothesized that PLL treatment targets the c-Myc pathway that can regulate the production of VEGF and angiogenesis. Thus, it is mechanistically clear how PLL can hinder angiogenesis as besides the c-Myc downregulation PLL also inhibited VEGF, VEGFR2 expression in BALB/c induced mice tumor.

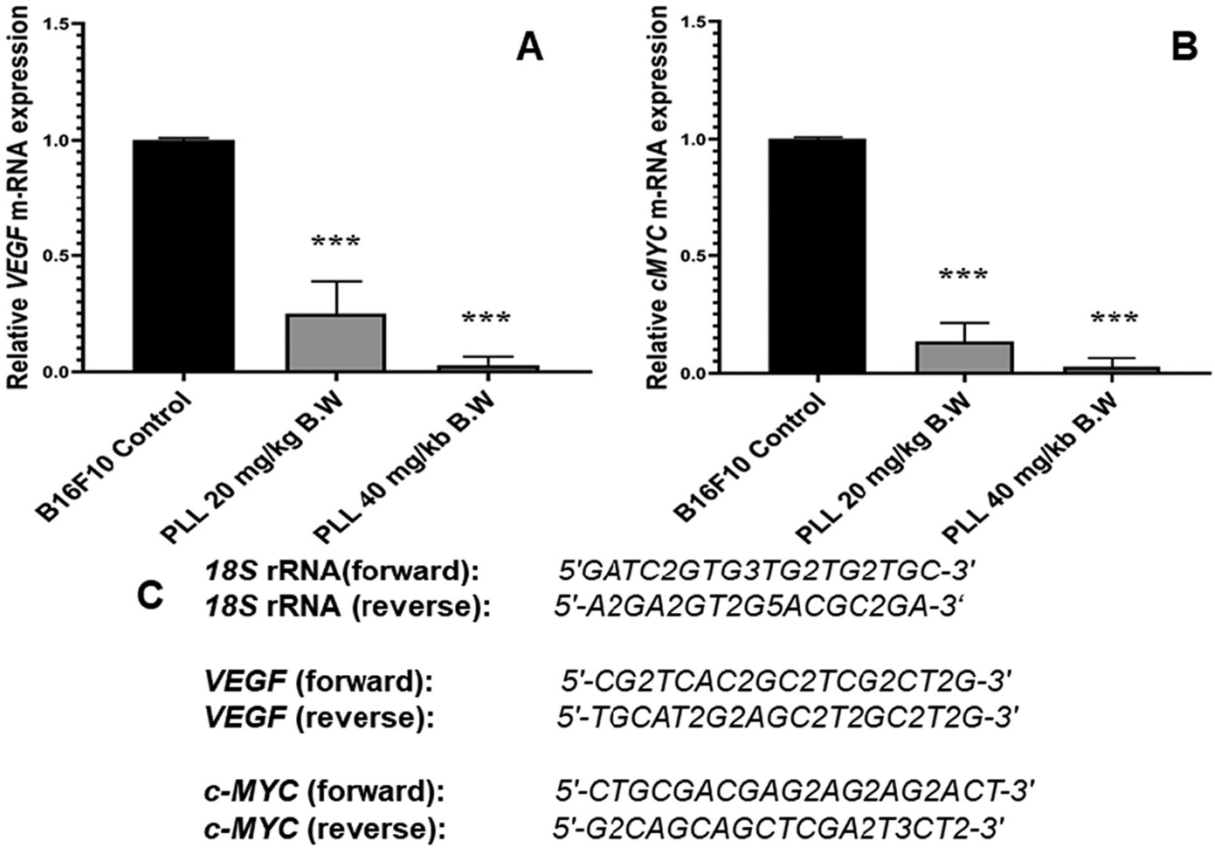

Fig. 16. Suppression of transcription level inB16F10 tumor cells results in downregulation of tumor-angiogenesis and proliferation markers. (A) and (B) Quantitative real-time polymerase chain reaction (RT-PCR) shows tumor-angiogenic and proliferation markers at the mRNA level with significant positive fold changes in the miRNA suppressed in the PLL treated B16F10 tumor cells compared with the control B16F10 tumor cells. Quantitative analysis of transcriptional level shows reduced levels of tumor-angiogenesis and proliferation markers *VEGF* and *c-Myc*. RT-PCR quantitative data are presented as the mean ± SEM of triplicate replicates; $^{***}P < 0.001$.

As it is well-known angiogenesis is defined as the formation of new blood vessel growth from existent microvessels and involves several processes, including the endothelial cell proliferation, proteolytic degradation of the extracellular matrix, and migration of endothelial cells, leading to the organization of endothelial cells into capillary-like structures [37,38]. Angiogenesis plays a pivotal role in tumor growth and metastasis has led to the development of anti-angiogenesis therapy for the treatment of solid tumors [39]. From this study, PLL was found to be a ley modulator of important proteins related to angiogenesis like c-Myc, VEGF, *etc.* In a more in-depth study, it was also found that PLL significantly reduced the microvessel density in the CAM model and also induced significant tumor growth inhibition in the BALB/c mouse model bearing B16F10 melanoma tumor cell. These data indicate that PLL might inhibit angiogenesis through the inhibition of VEGF-induced endothelial cell functions involved in angiogenesis.

Photomicrographs of all tumor sections excised from the BALB/c mice were stained with H&E. The sections were examined to quantify the blood vessels and viable and necrotic tissue. Histological sections of the tumors from negative control mice were full of growing tissue with plenty of viable cells arranged compactly and resembling the vigorous proliferation of cancerous cells [40]. Microscopic evaluation in higher magnification revealed that the viable tissue was composed of highly compact sheets of polygonal-shaped cells with prominent nuclei and numerous blood vessels. Either little or no necrotic areas were observed in the tissue sections of untreated mice. The tumors in the PLL treatments showed strong evidence of an anti-angiogenic effect. Due to reduced blood and oxygen supply, the tumors in PLL-treated animals exhibited loss of compactness of the viable cells with moderate to severe necrosis. The necrotic areas with a reduced density of viable cells are visible in the tumor sections. Small regions of viable tissue with cells can be seen in the treated tumor sections. Treatment with PLL resulted in significant anti-tumorigenic activity and a reduction in blood vessel density compared to the control group.

Usually, in cancer chemotherapy, the major problems that are encountered are myelosuppression and anaemia. It has been frequently observed in ascites carcinoma [41,42] and similar findings were also observed in our present study. In B16F10 control mice, elevated WBC count and reduced haemoglobin and RBC count were observed. Reduced haemoglobin encountered in ascites carcinoma mainly occurs due to iron deficiency, either by hemolytic or myelopathic conditions, which finally lead to reduced RBC number [43]. We observed that PLL treatment prevented the fall in haemoglobin content and maintained normal values of RBC and WBC in a dose-dependent manner. These indicating parameters revealed that PLLvery less toxic effect on the hemopoietic system and plausibly had a selective affinity to the tumor cell and thereby it could maintain the normal haematological profile. Treatment with PLL maintains the normal values of whole blood count, which supports its hematopoietic protecting activity. Induction of myelotoxicity in B16F10 bearing BALB/c mice is considered to be of immunological significance ice to meet the adverse situation developed by the introduction of foreign bodies in the blood [44].

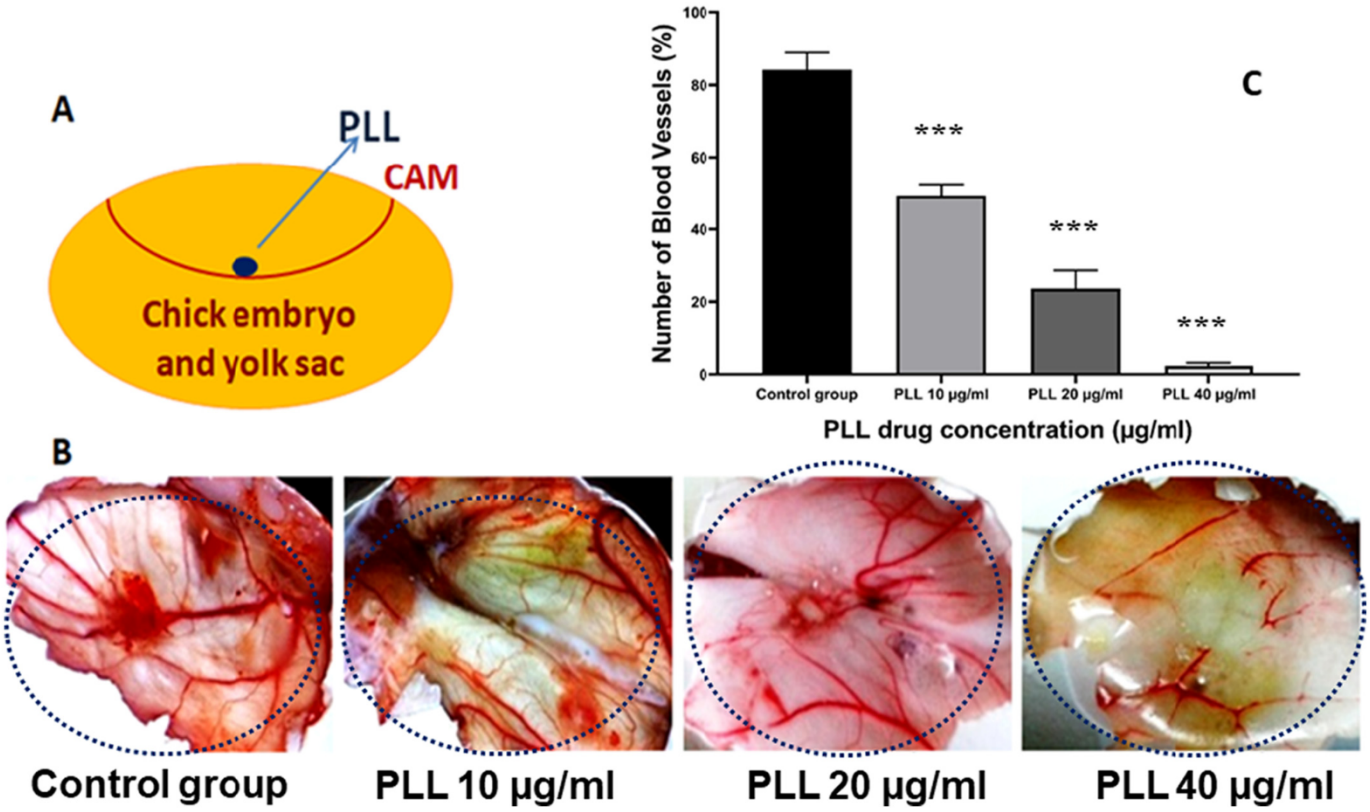

Fig. 17. PLL inhibits angiogenesis in a chick embryo CAM model. (A) CAM assay was used to determine the effects of PLL on the inhibition of angiogenesis. (B) Representative images show the appearance of blood vessels in chick embryo CAMs treated with 10, 20, and 30 µg/ml of PLL for 48 h. Pictures of PLL treatment show the avascular zone around where the PLL test drug was administered. The applied dose (µg/ml/CAM) and the anti-angiogenesis ratio are shown below the pictures. In the panel-B, showing the caliber of principal blood vessels; there were very fewer blood vessel branches in the PLL-treated CAMs than in the control group, where blood vessels were reduced dose-dependently. (C) Statistical analysis of the CAMs showed that PLL significantly reduced blood vessel density (MVD). ± SEM of triplicate replicates, $^{***}P < 0.001$.

Overall, these findings, particularly on the high selectivity of PLL on breast cancer cells and melanoma metastatic tumor cells and mechanism of action, may lead to further development of a potential anticancer drug. However, the molecular signalling pathways still requires further investigation. Thus, this study establishes that there is still room for improvement in designing modified formulation with increased anticancer activities. Overall, these findings are indicative of PLL induced extensive apoptosis of the tumor cells with vascular perfusion, reduced micro vessel density, and decreased tumorigenesis.

5. Conclusion

In a nutshell, the present study revealed that PLL was internalized in both epithelial MDA-MB-231 triple-negative breast cancer and murine melanoma B16F10 malignant tumor cells, in 2D monolayer cultures, 3D tumor spheroid model, and *in-vivo* BALB/c mice model.

Indeed, PLL was found to be a pro-apoptotic and anti-proliferative agent. At particular dosimetry, PLL was found to serve such function particularly in the 3D culture of MDA-MB-231 and in the B16F10 induced mice model.

Indeed, treatment indicated that PLL induced apoptotic cell death is mitochondria mediated and caspase-3 dependent. As a result of our study, the treated tumor cells upon PLL induction exhibited a major reduction in proliferation index. Further, the experimental outcome showed that PLL can effectively block the cell proliferation, tumor angiogenesis along with a higher percentage of cells associated with mitochondrial depolarization, cytochrome-C release followed by apoptosis. PLL reduced tumor growth of melanoma tumor cell *in-vivo* by down reregulation of VEGFR2 signalling. The molecular mechanism implies an association between the suppression of VEGF induced proliferation *via* activated caspase-3 and PARP. PLL induced downregulation of VEGF and c-Myc and the inhibition of Ki67 and CD34 indicates its potential as an antiproliferative agent. Alteration in VEGF expression both in *in-vitro* and *in-vivo* after PLL induction downregulates the vascular network also confirms its anti-angiogenic property. Therefore, our experiment suggests that the downregulation of c-Myc susceptibility and sensitivity by PLL towards downregulating tumor neovascularization and tumor proliferation help in the induction of intrinsic mitochondria mediated apoptosis and inhibition of tumor development and proliferation.

The main significance of our present study is that we have found PLL as a novel anticancer agent that has the potential to inhibition of tumor proliferation and induces apoptosis both in monolayer 2D and 3D physiological relevant tumor microenvironment. Along with this in conjunction with our previous study, we demonstrate that PLL also bears the property to block the angiogenic process *via* the downregulation of VEGF and c-Myc dependent pathway. Our study has proved that PLL significantly repressed *in-vitro* aggressive MDA-MB-231 breast cancer cells as well as in the *in-vivo* condition it was found that PLL block B16F10 induced tumorigenesis process in BALB/c mice through the caspase-3 and PARP activated mitochondrial intrinsic apoptotic pathway. PLL was also found to be an antiproliferative and anti-angiogenic compound that exerted such efficacy through the downregulation of Ki-67, VEGF, VEGFR2, and c-Myc gene expression level Fig. 18. Thus, this study indicates PLL as a potential therapeutic agent against multiple aggressive human malignancies.

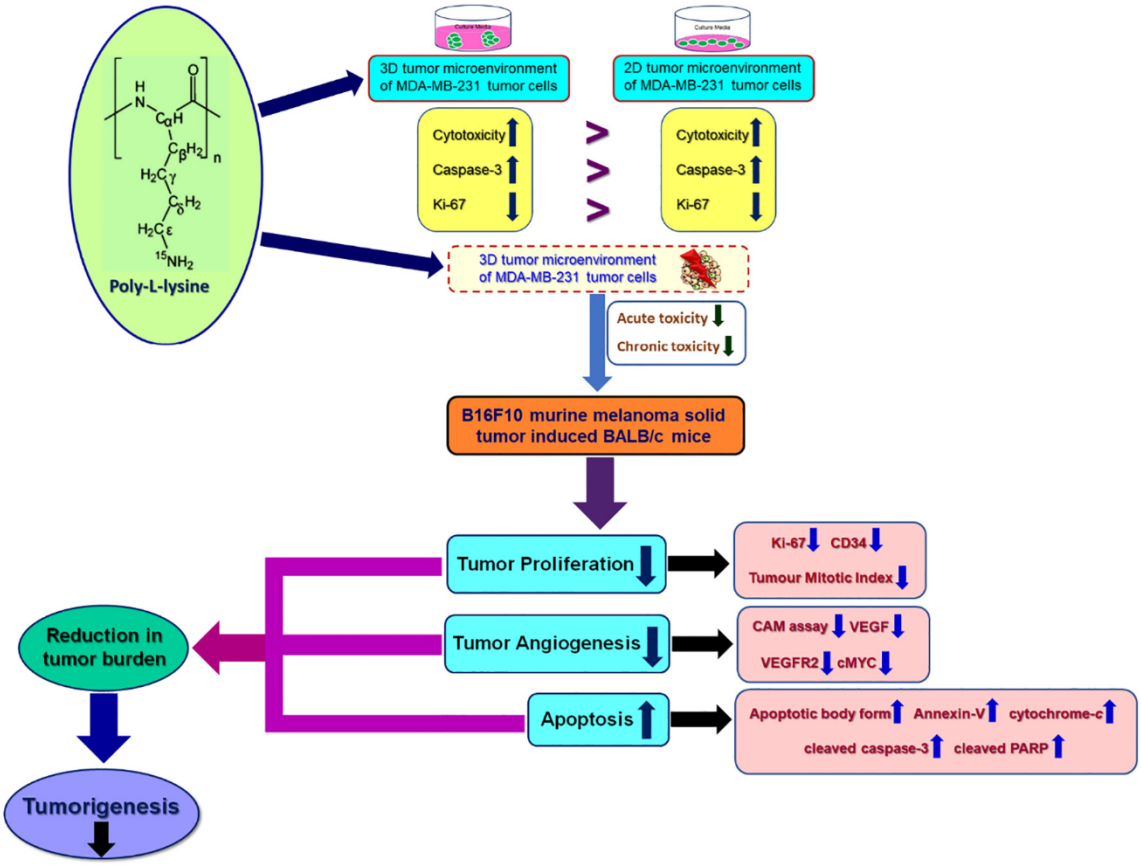

Fig. 18. Graphical abstract

Ethics approval and consent to participate

The study protocol was approved by the institutional animal ethical committee of Jadavpur University, Department of Pharmaceutical Technology, Kolkata, India. This research work was approved by the Ethical Review Committee of Research cell of Jadavpur University of Science and Technology, Kolkata-700,032, India (Registration number: 147/1999/CPCSEA).

Consent for publication

Not applicable.

Availability of data and materials

Data and materials are available upon request.

CRediT authorship contribution statement

Souvk Debnath conceptualized and performed the complete research work and wrote the complete manuscript. Avinaba Mukherjee and Dhananjoy Saha helped to data interpretation and revised the complete manuscript. Dhananjoy Saha, Jyotirmayee Dash and Tapan Kumar Chatterjee guiding through the whole work and during the writing of research article and revised the final manuscripts. All authors have read and approved the final manuscript.

Declaration of competing interest

The authors declare that they have no conflict of interest.

Acknowledgements

This work was also supported by a grant from the Science and Engineering Research Board (SERB) of India sanctioned to Souvik Debnath through SERB-OVDF at Purdue University, USA in collaboration with Jadavpur University, India through Overseas Visiting Doctoral Research Fellowship scheme, New Delhi, India [SB/S9/Z-03/2017-III] (2019–2020).

Funding

This work was supported by a grant from the Science and Engineering Research Board (SERB) of India sanctioned to Souvik Debnath through SERB-OVDF at Purdue University, USA in collaboration with Jadavpur University, India through Overseas Visiting Doctoral Research Fellowship scheme, New Delhi, India [SB/S9/Z-03/2017-III] (2019-2020).

References

[1] R.L. Siegel, K.D. Miller, A. Goding Sauer, S.A. Fedewa, L.F. Butterly, J.C. Anderson, A. Cercek, R.A. Smith, A. Jemal, Colorectal cancer statistics, CA Cancer J. Clin. 70 (3) (2020) 145–164.
[2] Wouter C. Meijers, Rudolf A. de Boer, Common risk factors for heart failure and cancer, s.l. Cardiovasc. Res. 115 (5) (2019) 844–853.
[3] J. Ferlay, H.R. Shin, F. Bray, D. Forman, C. Mathers, D.M. Parkin, Estimates of worldwide burden of cancer in 2008: GLOBOCAN 2008, Int. J. Cancer 127 (12) (2010) 2893–2917.
[4] L.A. Torre, R.L. Siegel, E.M. Ward, A. Jemal, Global cancer incidence and mortality rates and trends—an update, Cancer Epidemiology and Prevention Biomarkers 25 (1) (Dec 14 2015) 16–27.
[5] E. Chatelut, J.P. Delord, P. Canal, Toxicity patterns of cytotoxic drugs, Investig. New Drugs 21 (2) (2003 May) 141–148.

[6] Ambili Remesha, Toxicities of anticancer drugs and its management, s.l International Journal of Basic & Clinical Pharmacology 1 (1) (2012) 2.
[7] Maria J. Bueno, Silvana Mouron, Miguel Quintela-Fandino, Personalising and targeting antiangiogenic resistance: a complex and multifactorial approach, Br. J. Cancer 116 (9) (2017) 1119.
[8] Naveen S. Vasudev, Andrew R. Reynolds, Anti-angiogenic therapy for cancer: current progress, unresolved questions and future directions, Angiogenesis 17 (3) (2014) 471–494 17.3 (2014): 471-494.
[9] Robert S. Kerbel, Tumor angiogenesis, N. Engl. J. Med. 358 (19) (2008) 2039–2049.
[10] Melissa García-Caballero, et al., The natural antiangiogenic compound AD0157 induces caspase-dependent apoptosis in human myeloid leukemia cells, Front. Pharmacol. 8 (2017) 802.
[11] Naoyo Nishida, et al., Angiogenesis in cancer, Vasc. Health Risk Manag. 2.3 (2006) 213.
[12] Yihai Cao, Future options of anti-angiogenic cancer therapy, Chinese journal of cancer 35 (1) (2016), 21.
[13] Judah Folkman, Angiogenesis and apoptosis, s.l. : Academic Press Semin. Cancer Biol. 13 (2003) 159–167.
[14] S. Debnath, S. Karan, M. Debnath, J. Dash, T.K. Chatterjee, Poly-L-lysine inhibits tumor angiogenesis and induces apoptosis in Ehrlich ascites carcinoma and in sarcoma S-180 tumor, Asian Pacific journal of cancer prevention: APJCP. 18 (8) (2017) 2255.
[15] Souvik Debnath, et al., Induction of apoptosis, anti-proliferation, tumor-angiogenic suppression and down-regulation of Dalton's Ascitic Lymphoma (DAL) induced tumorigenesis by poly-l-lysine: a mechanistic study, Biomed. Pharmacother. 102 (2018) 1064–1076.
[16] Souvik Debnath, et al., The therapeutic value of lysine against cance: a comprehensive review, International Journal of Biology, Pharmacy and Allied Sciences (IJBPAS) 9 (2020) 3218–3247.
[17] Jessica Hoarau-Véchot, et al., Halfway between 2D and animal models: are 3D cultures the ideal tool to study cancer-microenvironment interactions? Int. J. Mol. Sci. 19.1 (2018) 181.
[18] Donglai Lv, et al., Three-dimensional cell culture: a powerful tool in tumor research and drug discovery, Oncol. Lett. 14.6 (2017) 6999–7010.
[19] Styliani Melissaridou, et al., The effect of 2D and 3D cell cultures on treatment response, EMT profile and stem cell features in head and neck cancer, Cancer Cell Int. 19.1 (2019) 16.
[20] Daniel S. Reynolds, et al., Breast cancer spheroids reveal a differential cancer stem cell response to chemotherapeutic treatment, Sci. Rep. 7.1 (2017) 1–12.
[21] Ana S. Nunes, et al., 3D tumor spheroids as in vitro models to mimic in vivo human solid tumors resistance to therapeutic drugs, Biotechnol. Bioeng. 116 (1) (2019) 206–226.
[22] M.J. Paszek, N. Zahir, K.R. Johnson, J.N. Lakins, G.I. Rozenberg, A. Gefen, C.A. Reinhart-King, S.S. Margulies, M. Dembo, D. Boettiger, D.A. Hammer, Tensional homeostasis and the malignant phenotype, Cancer Cell 8 (3) (2005) 241–254.
[23] Andrea Sadlonova, et al., Breast fibroblasts modulate epithelial cell proliferation in three-dimensional in vitro co-culture, Breast Cancer Res. 7 (1) (2004) R46.
[24] Silva Krause, et al., A novel 3D in vitro culture model to study stromal–epithelial interactions in the mammary gland, Tissue Engineering Part C: Methods 14 (3) (2008) 261–271.
[25] Aja M. Rieger, et al., Modified annexin V/propidium iodide apoptosis assay for accurate assessment of cell death, JoVE (Journal of Visualized Experiments) 50 (2011) e2597.
[26] C. Garrido, et al., Mechanisms of cytochrome c release from mitochondria, s.l. Cell Death Differ. 13 (9) (2006) 1423–1433.
[27] G.M. Cooper, The Cell: A Molecular Approach, 2nd edition, The Development and Causes of Cancer, , Sinauer Associates, Sunderland (MA), 2000.
[28] Clémence Dubois, et al., Development and cytotoxic response of two proliferative MDA-MB-231 and non-proliferative SUM1315 three-dimensional cell culture models of triple-negative basal-like breast cancer cell lines, Oncotarget 8 (56) (2017) 95316.
[29] Yanfang Ding, et al., Three-dimensional tissue culture model of human breast cancer for the evaluation of multidrug resistance, J. Tissue Eng. Regen. Med. 12 (9) (2018) 1959–1971.
[30] R.K. Singh, A. Ranjan, A.K. Srivastava, M. Singh, A.K. Shukla, N. Atri, A. Mishra, A.K. Singh, S.K. Singh, Cytotoxic and apoptotic inducing activity of Amoora rohituka leaf extracts in human breast cancer cells, J. Ayurveda Integr. Med. 11 (4) (2020) 383–390.
[31] Shao-Ju Jin, et al., In vivo and in vitro induction of the apoptotic effects of oxysophoridine on colorectal cancer cells via the Bcl-2/Bax/caspase-3 signaling pathway, Oncol. Lett. 14 (6) (2017) 8000–8006.
[32] Fernanda Faiao-Flores, et al., Apoptosis through Bcl-2/Bax and cleaved caspase upregulation in melanoma treated by boron neutron capture therapy, PLoS One 8 (3) (2013).
[33] c-Myc and cancer metabolism." Miller, Donald M., et al. ". (2012): , pp. 5546–5553.
[34] D.J. Liao, R.B. Dickson, c-Myc in breast cancer, Endocr. Relat. Cancer 7 (3) (2000) 143–164.
[35] Guanhua Song, et al., c-myc but not Hif-1α-dependent downregulation of VEGF influences the proliferation and differentiation of HL-60 cells induced by ATRA, Oncol. Rep. 29 (6) (2013) 2378–2384.
[36] Testini, Chiara, et al., (Eds.),EMBO Rep. 20 (11) (2019).
[37] Arno Amann, et al., Development of a 3D angiogenesis model to study tumour–endothelial cell interactions and the effects of anti-angiogenic drugs, Sci. Rep. 7 (1) (2017) 1–13.
[38] D.M. Form, B.M. Pratt, J.A. Madri, Endothelial cell proliferation during angiogenesis. In vitro modulation by basement membrane components, Labo. Invest. 55 (5) (1986) 521–530.
[39] Hueso, Luisa, et al., (Eds.),Dynamics and implications of circulating anti-angiogenic VEGF-A 165 b isoform in patients with ST-elevation myocardial infarction, Sci. Rep. 7 (1) (2017) 9962.
[40] Friedrich Foerster, et al., Enhanced protection of C57 BL/6 vs Balb/c mice to melanoma liver metastasis is mediated by NK cells." Foerster, Friedrich, et al. "Enhanced protection of C57 BL/6 vs Balb/c mice to melanoma liver metastasis is mediated by NK cells, Oncoimmunology 7 (4) (2018), e1409929, (2018): , Oncoimmunology , Vol. 7.4, p. e1409929).
[41] Kumar, Dhiraj, et al., (Eds.),BMC Cancer 18 (1) (2018) 52.
[42] V.E. Price, R.E. Greenfield, Anemia in cancer, s.l. : Academic Press InAdvances in cancer research 5 (1958) 199–290.
[43] F. Islam, S. Ghosh, J.A. Khanam, Antiproliferative and hepatoprotective activity of metabolites from Corynebacterium xerosis against Ehrlich ascites carcinoma cells, May 1;4 Asian Pac. J. Trop. Biomed. (2014) S284–S292.
[44] M.A. El-Magd, A. Khamis, S.K. Eldeen, W.M. Ibrahim, A.F. Salama, Trehalose enhances the antitumor potential of methotrexate against mice bearing Ehrlich ascites carcinoma, Biomed. Pharmacother. 92 (Aug 1) (2017) 870–878.